SYNTHESIS AND MODIFICATION OF TITANOSILICATE ETS-10: ITS ROLE AS HOST IN HOST-GUEST SYSTEMS

A THESIS SUBMITTED TO
THE GRADUATE SCHOOL OF NATURAL AND APPLIED SCIENCES
OF
MIDDLE EAST TECHNICAL UNIVERSITY

BY
MELDA İŞLER

IN PARTIAL FULLFILLMENT OF THE REQUIREMENTS
FOR
THE DEGREE OF MASTER OF SCIENCE
IN
MICRO AND NANOTECHNOLOGY

FEBRUARY 2014

Approval of the thesis:

SYNTHESIS AND MODIFICATION OF TITANOSILICATE ETS-10: ITS ROLE AS HOST IN HOST-GUEST SYSTEMS

submitted by **MELDA İŞLER** in partial fulfillment of the requirements for the degree of **Master of Science in Micro and Nanotechnology Department, Middle East Technical University** by,

Prof. Dr. Canan Özgen
Dean, Graduate School of **Natural and Applied Sciences** _______________

Prof. Dr. Tayfun Akın
Head of Department, **Micro and Nanotechnology** _______________

Assoc. Prof. Dr. Burcu Akata Kurç
Supervisor, **Micro and Nanotechnology Dept., METU** _______________

Prof. Dr. Raşit Turan
Co-Supervisor, **Physics Department, METU** _______________

Examining Committee Members:

Prof. Dr. Hayrettin Yücel
Chemical Eng. Department, METU _______________

Assoc. Prof. Dr. Burcu Akata Kurç
Micro and Nanotechnology Department, METU _______________

Assoc. Prof. Dr. Can Özen
Biotechnology Department, METU _______________

Assoc. Prof. Dr. Ali Çırpan
Chemistry Department, METU _______________

Dr. Kemal Behlülgil
Central Laboratory, METU _______________

Date: _______________

I hereby declare that all information in this document has been obtained and presented in accordance with academic rules and ethical conduct. I also declare that, as required by these rules and conduct, I have fully cited and referenced all material and results that are not original to this work.

Name, Last Name: MELDA İŞLER

Signature :

ABSTRACT

SYNTHESIS AND MODIFICATION OF TITANOSILICATE ETS-10: ITS ROLE AS HOST IN HOST-GUEST SYSTEMS

İŞLER, Melda

M.Sc., Department of Micro and Nanotechnology
Supervisor : Assoc. Prof. Dr. Burcu Akata Kurç
Co-Supervisor : Prof. Dr. Raşit Turan

February 2014, 84 Pages

An attractive method to create new molecular level electronic, optical and magnetic devices is to use solid host lattices that serve as templates within which a guest structure of nanometer architecture can be assembled. Zeolites and zeo-type materials with nanopores and cavities in 3-dimensions are known to represent a “New Frontier” of solid state chemistry with great opportunities for innovative research. Titanosilicate ETS-10, a microporous material, possessing two perpendicular channels, is an alternative, promising zeo-type material for host-guest systems with its most intriguing property of possessing two dimensional Ti-O-Ti quantum wires with semiconductor properties.

Furthermore, it is critical to control concentration and type of defects inside zeolite crystals in order to enhance diffusion access through three dimensional pore systems for host-guest systems. An approach to form defects; i.e. intracrystalline mesoporosity, can be obtained by post-synthesis modification.

In the current study, the aim was to investigate synthesis of ETS-10 crystals possessing several morphologies and host-guest systems in which ETS-10 was used as a host material and ruthenium nanoparticles as well as dye molecules as guest materials. ETS-10 crystals were synthesized with various molar compositions in order to achieve ETS-10 crystals with desired morphology. Some of the ETS-10 nanocrystals were modified by post-synthesis methods; i.e. consecutive hydrogen peroxide and sulfuric acid treatments.

Secondly, ETS-10 crystals that were subjected to the above mentioned post-synthesis modifications and those that were not modified were investigated as host material by incorporating nanoparticles or dye molecules. For the investigation of ETS-10 as a host material for metallic nanoparticles, ruthenium nanoparticles were aimed to be incorporated into both as-synthesized and post-treated ETS-10 crystals. The resulting ETS-10 crystals were characterized by XRD, FE-SEM, ICP-MS, HR-TEM and N_2 adsorption/desorption methods in order to comprehend the effect of defects formed by post-treatments in ruthenium nanoparticle formation in ETS-10 matrix.

As an alternative to metallic nanoparticle formation, ship-in-a-bottle synthesis of a ruthenium based dye molecule, that is of high demand in photovoltaic studies was sought to be formed in the ETS-10 matrix. For this purpose, tris(2,2’-bipyridiyl)ruthenium(II) cation, an organometallic dye molecule, was incorporated with the ETS-10 matrix for the first time. The characterization of tris(2,2’-bipyridiyl)ruthenium(II) cation incorporated into ETS-10 was performed by FT-IR, UV-Vis spectroscopy and CLSM. Furthermore, pyronine as a small linear molecule was loaded into ETS-10 and characterized by CLSM in order to observe the diffusion of a small cationic dye into ETS-10 as an alternative.

Keywords: ETS-10, Modification in Structure of ETS-10, Host-Guest Systems, Ruthenium Nanoparticles, Ship-in-a-bottle Synthesis.

ÖZ

TİTANYUMSİLİKAT ETS-10 SENTEZİ VE MODİFİKASYONU: KONUK-KONAK SİSTEMLERDE KONAK OLARAK ROLÜ

İŞLER, Melda

Yüksek Lisans, Mikro ve Nanoteknoloji Bölümü

Tez Yöneticisi: Doç. Dr. Burcu Akata Kurç

Ortak Tez Yöneticisi: Prof. Dr. Raşit Turan

Şubat 2014, 84 sayfa

Yeni moleküler düzeyde elektronik, optik ve magnetik cihazlar üretebilmek için, konuk-konak sistemlerinde nanometrik ölçekteki konuğu barındarıbilen katı konak matrisleri kullanmak ilgi çekici bir yöntemdir. 3 boyutlu nanogözenek ve boşuklara sahip olan zeolit ve zeo-tip malzemeler, yenilikçi araştırmalar için büyük imkanlara sahip olmasıyla katıhal kimyasında "yeni bir hudud"u temsil ettikleri bilinmektedir. Birbirine dik iki kanala sahip olan mikrogözenekli titanyumsilikat ETS-10, en ilgi çekici özelliği olan iki boyutlu yarı-iletken Ti-O-Ti zincirine sahip olmasıyla konuk-konak sistemler için alternatif umut veren zeo-tip bir malzemedir.

Ayrıca, konuk-konak sistemlerde 3 boyutlu gözeneklerden difüzyonu geliştirebilmek için zeolit kristalindeki kusurların konsantrasyonunu ve türünü kontrol etmek son derece önemlidir. Sentez-sonrası işlem, kristalde kusur oluşturmak için alternatif bir yöntemdir.

Bu çalışmada, değişik morfolojilere sahip ETS-10 sentezlemek ve ETS-10'nin konak, boya veya rutenyum nanoparçacıkların konuk olduğu konuk-konak sistemlerini incelemek amaçlanmıştır. İstenen morfolojiye ulaşabilmek için farklı molar kompozisyona sahip ETS-10 kristalleri sentezlendi ve sentezlenen ETS-10 kristallerinin bir kısmı sentez-sonrası işlem ile yani sırasıyla, hidrojen peroksit ve sülfürik asit ile modifiye edildi.

İkinci olarak yukarda bahsedilen, sentez-sonrası işleme maruz bırakılmış ve bırakılmamış ETS-10 kristallerinde, nanoparçacık veya boya molekülleri oluşturularak ETS-10 konak olarak incelenmiştir. Konak olarak ETS-10, sentez-sonrası işlem maruz bırakılmış ve bırakılmamış ETS-10 kristallerinde rutenyum nanoparçacık sentezlenerek ilk olarak incelenmiştir. Sentez-sonrası işlemin, ETS-10 matrisindeki nanoparçacık oluşumuna etkilerini daha iyi anlayabilmek adına X-Işını Kırınım Cihazı (XRD), Taramalı Elektron Mikroskobu (SEM), Endüktif Eşleşmiş Plazma Spektroskopisi (ICP-MS), Tünelleme Elektron Mikroskobu (TEM) ve N_2 Adsorpsiyon Tekniği kullanılmıştır.

Metalik nanoparçacık oluşumuna ek olarak, fotovoltaik çalışmalarda büyük rağbet gören rutenyum bazlı boya molekülü, tris(2,2'-bipiridil)rutenyum (II) katyonu, ilk defa ETS-10 matrisinde "şişe içinde gemi" sentezi yöntemiyle sentezlenmiştir. ETS-10 ile birleşik tris(2,2'-bipiridil)rutenyum (II) katyonu FT-IR, UV-Vis Spektroskopileri ve Konfokal Lazer Taramalı Mikroskobu (CLSM) ile karakterize edilmiştir. Bunun yanısıra, alternatif olarak, küçük düzlemesel yapıya sahip olan pironin boya molekülleri, ETS-10 kristalleri içine yüklenmiştir ve bu yapının karakterizasyonu CLSM ile yapılmıştır.

Keywords: ETS-10, ETS-10 Kristallerinin Modifikasyonu, Konuk-Konak Sistemleri, Rutenyum Nanoparçacık, Şişe-içinde-gemi Sentezi.

to my family…

ACKNOWLEDGEMENTS

It gives me great pleasure to express my sincere gratitude to my advisor Assoc. Prof. Dr. Burcu Akata Kurç, for her support, inspiration, and guidance during my M.Sc. study. Her trust in me has changed all my academic life.

Furthermore, I would like to thank to the rest of my thesis committee; Prof. Dr. Hayrettin Yücel, Assoc. Prof. Dr. Ali Çırpan, Assoc. Prof. Dr. Can Özen, and Dr. Kemal Behlülgil for their precious comments.

I would also like to thank to METU Central Laboratory, for enabling its wide facilities anytime needed in this work. Also I would like to thank to group members; Sezin Galioğlu, Berna Ozansoy Kasap, Duygu Kuzyaka, Kaan Kirdeciler, Mehmet Koç, Seçkin Öztürk and Sedat Canlı for their friendship and helps during my study. All of them calmed me down when I was stressed out, and they helped me sincerely when I was in trouble. I would also like to thank Prof. Dr. Saim Özkar and Serdar Akbayrak for their guidance and help in the UV-Vis Spectroscopy analysis in METU Chemistry Department. I would also thank Can Özen and Efe Erdeş for support in Confocal Laser Scanning Microscopy. I would like to thank Merve Cengiz Çerçi, İlker Yıldız, Serap Tekin, Sezen Yıldırım, Özgür Erişen, Uğur Özgürgil and Levent Yıldız for their supports in Central Laboratory. I would also like to thank Serdar Sezer and Ümran Aydemir Sezer for their guidance, inspiration and supports.

The author is most grateful to her family members for supporting her continuously throughout her life unconditionally, to her mother, for raising her with never-ending love, patience and support, to her father, for teaching her the excitement of science and committing his life to his family, to her sister Bihter İşler, for their love, never-ending patience and support.

Last but not least, I would like to give my endless gratitude to Emrah Binay, who supported and motivated me with his love and understanding during the whole period of my study.

TABLE OF CONTENTS

APPENDICES

LIST OF TABLES

TABLES

LIST OF FIGURES

FIGURES

LIST OF ABBREVIATION

ETS: Engelhard Titanosilicate

SEM: Scanning Electron Microscopy

HR-TEM: High Resolution Transmission Electron Microscopy

ICP-MS: Inductively Coupled Plasma – Mass Spectrophotometer

XRD: X-Ray Diffraction

CLSM: Confocal Laser Scanning Microscopy

CHAPTER 1

INTRODUCTION

1.1 Zeolites and Zeo-type materials

Zeolites and zeo-type materials having a crystalline structure and framework linked tetrahedra units comprise open cavities in the forms of channels with well-defined acidity, good thermal stability and cation exchange selectivity. Their porous structure and cationic nature makes these unique materials suitable for ion exchange, adsorption and catalysis [1].

Zeolites consist of crystalline aluminosilicates with corner-sharing TO_4 tetrahedra. These regular tetrahedra sequences form three-dimensional frameworks containing uniform pore sizes. T-atoms are basically Si and Al; however, other metals such as P, Ga, Ge, and Ti can be used for the formation of zeolites [2]. Each T-atom is coordinated by four oxygen atoms from tetrahedral sites and each oxygen atom is bonded to two T-atom as seen Figure 1.1.

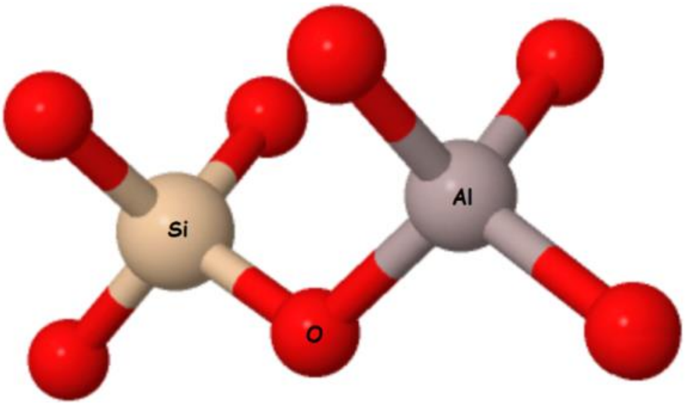

Figure 1.1. The connection of primary building units of zeolites; i.e. SiO_4 and AlO_4.

The zeolite framework consists of SiO_4 and AlO_4 tetrahedra. AlO_4 tetrahedra have an anionic framework character, which is stabilized by extra-framework cations. The general empirical formula can be represented as

$$M_{y/n}^{n+}\,[(SiO_2)_x\,.\,(AlO_2^-)_y]\,.\,z\,H_2O \qquad (1.1)$$

where M is an extra-framework cation with n^+ charge.

The extra-framework cations, which are responsible for balancing the structure, are electrostatically bonded to the framework, which let zeolite become advantageous for numerous applications. The most widespread and plentiful applications of zeolites are ion-exchange, selective sorption, and catalysis [3]. Also, rigid and porous structures of zeolites enable incorporating novel molecules such as nanoparticles and conductive polymers in zeolite matrix in order to enhance optical or conductive properties of these materials. For such a host-guest assembly systems, zeolite L and zeolite Y are the most common examples. Moreover, ETS-10, a titanosilicate microporous material, can be an alternative host for host-guest systems with its unique properties

1.1.1 ETS-10

ETS-10, a microporous titanosilicate with composition of $(Na,K)_2TiSi_5O_{13}.nH2O$, consists of corner-sharing SiO_4 tetrahedra and TiO_6 octahedra connected with bridging oxygen atoms [4-6]. The pore system comprises 12-membered rings and two perpendicular channels letting other molecules penetrate through the pores, possessing pore size with is 4.9 x 7.6 Å [9, 10]. Having TiO_3^{2-} quantum wires; which elongates through *a* and *b* axes shown in Figure 1.2 [11], let ETS-10 arise usage as photochemical and thermal reaction catalysis [8, 10, 11], photovoltaic solar cell [12] and nanoscale electronic devices [13].

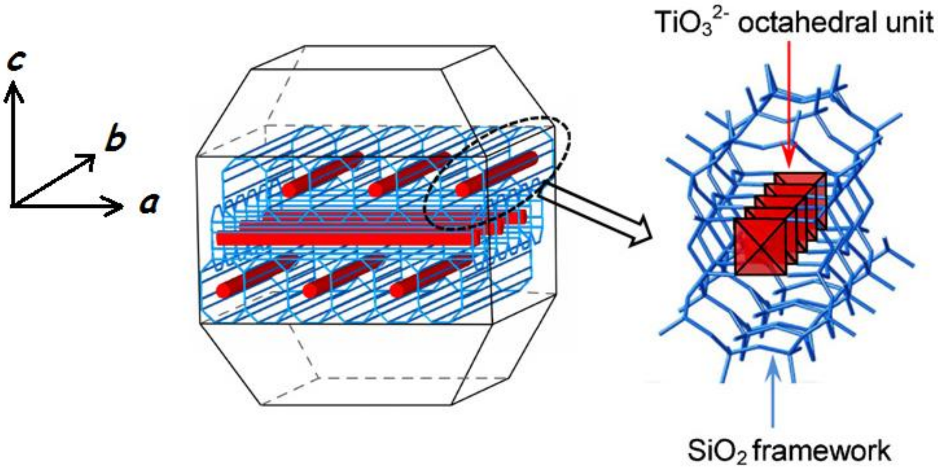

Figure 1.2. Schematic representation of ETS-10 crystals possessing a truncated bipyramidal shape. SiO_2 channels and TiO_3^{2-} quantum wires are represented with blue and red colors, respectively [9].

1.1.2 Zeolite Y

Zeolite Y is one of the members of Faujasite (FAU) type zeolites; which possesses supercages; i.e. α cages, with 1.3 nm and sodalite cages; i.e. β cages, with 0.74 nm as seen in Figure 1.2. The difference between zeolite Y and other FAU group members is the Si/Al ratio; which is 2.2-3 for zeolite Y [14]. Due to the pore structure of zeolite Y, encapsulation of guest molecules in larger cages; i.e. supercages, without any leaching through smaller cages; i.e. sodalite cages, is possible [15].

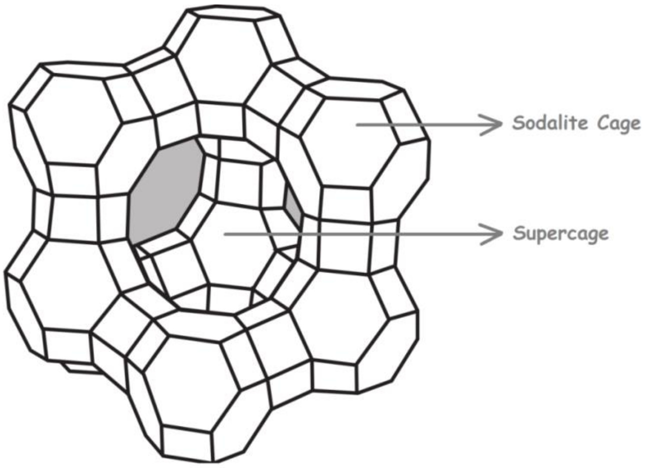

Figure 1.3. Representation of zeolite Y, possessing sodalite cages and supercages. (Adapted from [16].)

1.2 Zeolites as host materials

The use of zeolites and zeo-type materials as host materials is attractive due to their characteristics of well-defined, uniform pore size and improved chemical, thermal and mechanical properties. Since the channels and pores of zeolites are in the lower range of nanometer scale, the guest incorporated into zeolites must also in be nanometer scale, and this opens the possibility of selective sorption in zeolites. Different types of zeolites having various pore structures and morphologies can be incorporated with metal nanoparticles and/or metal complexes for forming host-guest systems with desirable properties [17].

1.3 Metal nanoparticles as guest material

Nobel metal nanoparticles possess extensive applications such as biosensing [18, 19] and catalytic applications [20, 21] due to their specific surface plasmon resonance. For such applications, agglomeration of metallic nanoparticles can be a disadvantage during the formation nanoparticles. For instance, surface plasmon resonance of nanoparticle can be varied by changing the particle's shape and volume, which should be kept under control for optical applications [22]. Furthermore, agglomeration of nanoparticles influences catalytic reactions negatively [23]. Thus it is critical to control such properties during nanoparticle formation in order to obtain desirable products [24]. Zeolites provide a matrix to prevent nanoparticles from agglomeration. Consequently, incorporation metal nanoparticles such as ruthenium nanoparticles into zeolites can be very interesting to minimize agglomeration of nanoparticles and also enhance the catalytic activity [23-25].

1.4 Dye molecules as guest material

Agglomeration is a critical problem for not only nanoparticles but also dye molecules in nanometer scale. In solution, dye molecules tend to agglomerate even at low concentrations. Dispersion of dye molecules in zeolite matrix can prevent dye molecules from agglomeration. Moreover, they are usually unstable to irradiation under many circumstances. The excited state energy of dye molecules is ready to be released as thermal relaxation. Incorporation of dye molecules into zeolite framework provides not only avoiding agglomeration but also fast thermal relaxation. Thus it unique optical activities of dye molecules such as light harvesting and transport can be observed by being incorporated into zeolite matrix [26-28].

Metal complexes, one of the member of dye molecules, are attractive as guest for host-guest assembly. Metal complexes incorporated into zeolites can be used as oxygen sensors [29] and electroluminescent cells [30]. Most specifically, metal polyamine complexes such as tris(2,2′-bipyridyl)ruthenium(II) cation are generally photoactive material, which allows them to be used in many applications such as photocatalyzed oxidation [31, 32] and photoinduced electron transfer reactions [33-36].

1.4.1 Tris(2,2′-bipyridyl)ruthenium(II) cation

Tris(2,2′-bipyridyl)ruthenium(II) cation; i.e. $[Ru(bpy)_3]^{2+}$, is one of the most widely used complex for photoactive applications due to its chemical stability and unique luminescence properties. The spectroscopic properties of $[Ru(bpy)_3]^{2+}$ can be arranged by altering its environment [37]. Thus, incorporation of $[Ru(bpy)_3]^{2+}$, with a spherical shape having 1.2 nm diameter as seen in Figure 1.4, into zeolites/zeo-type materials suggests can be used as an alternative material in optic and catalytic applications [30, 38]

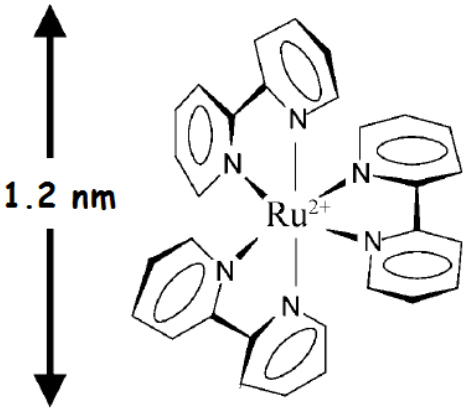

Figure 1.4. The chemical structure of $[Ru(bpy)_3]^{2+}$[39].

CHAPTER 2

LITERATURE SUMMARY

2.1 Zeolites and Zeo-type Materials

2.1.1 Synthesis of Zeolites and Zeo-type Materials

The major synthesis components are aluminum, silicon and alkali sources for zeolites; or titanium and vanadium for zeo-type materials. The size of zeolite crystals are strongly affected by the chemical sources used during synthesis. Control in the size/length of ETS-10 is discussed below.

Synthesis of ETS-10 with different chemical sources and chemical formulas has also been studied more than decades. Ji *et al*. [40], reported that changing the Na_2O/K_2O ratio and also water content affect the formation of as-synthesized ETS-10. Figure 2.1 indicates the change in morphology with water amount in reaction gel. It was reported that the water amount used in the reaction gel resulted in an increase in the size of ETS-10 along *a* and *b* directions and this did not result any change in *c* direction.

.

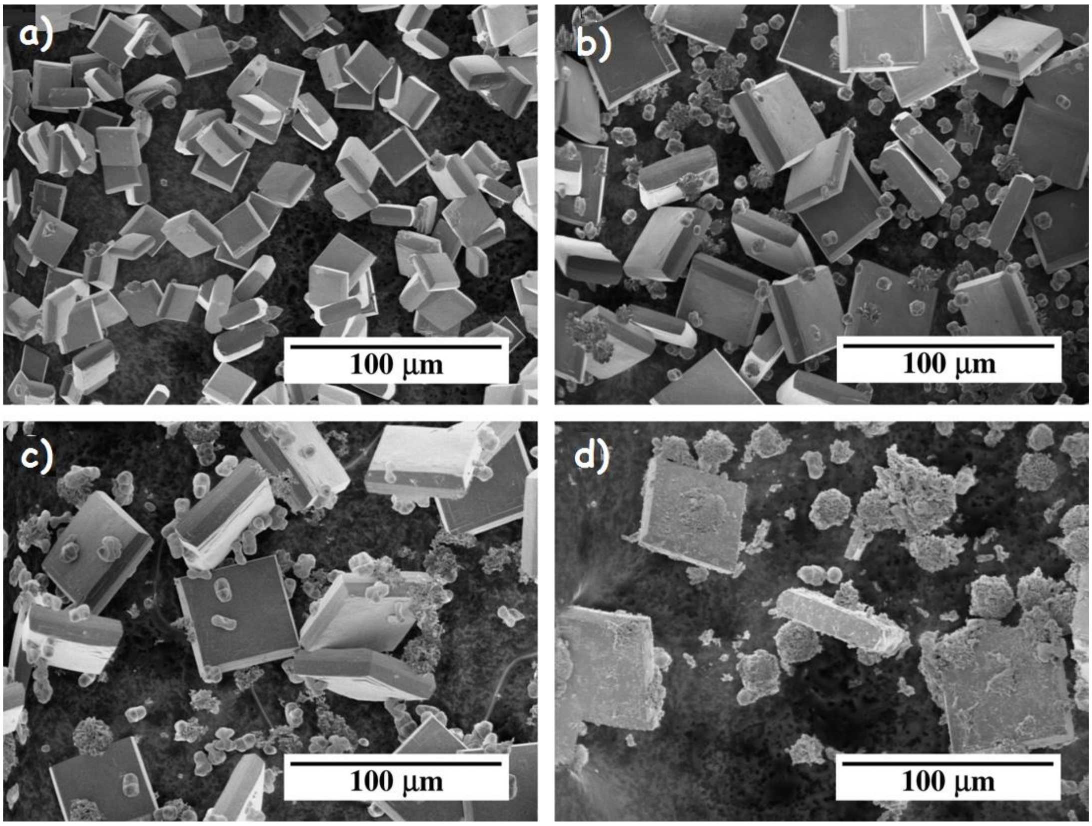

Figure 2.1. FE-SEM images of ETS-10 crystals synthesized hydrothermally with molar composition of $5.5SiO_2 : 2.97Na_2O : 1.49K_2O : TiO_2 : nH_2O$, where n = 300 (a), n = 500 (b), n = 750 (c), and n = 900 (d) [40].

Another remarkable research about ETS-10 is the effect of potassium fluoride on the morphology. Datta *et al.* [41] determined the length of *a* and *c* directions with altering fluoride content in the reaction gel. Figure 2.2 shows SEM images of products having different amount of fluoride ion. . As shown in Figure 2.2, as KF (n) amount decreases in the reaction gel from 2.48, to 2.01, 1.38, 0.92, 0.46, and to 0.09, *a* direction increases from 17 to 25, 32, 42, 50 and to 55 µm. Moreover, it was reported that all the products are highly crystalline and there is almost no impurity as indicated by SEM images.

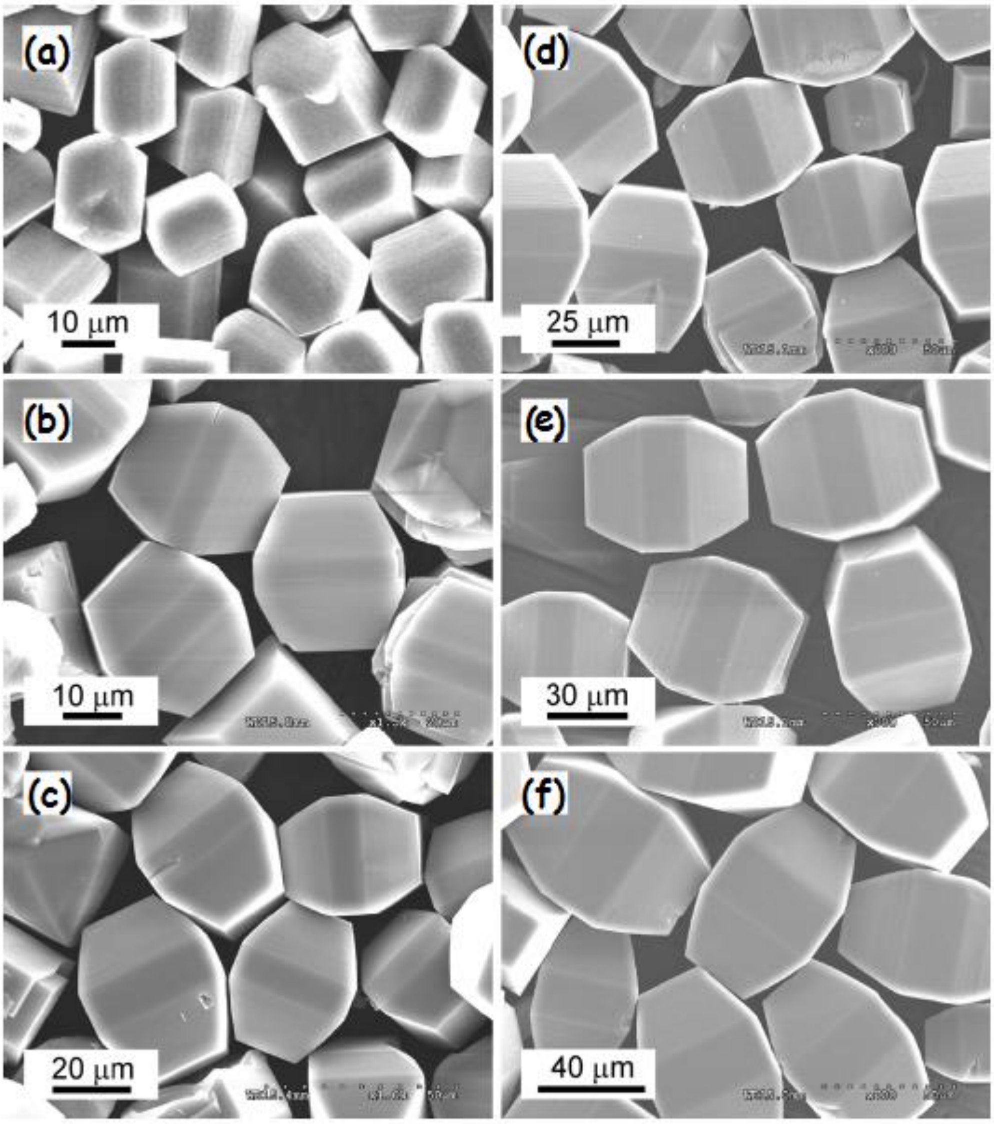

Figure 2.2. FE-SEM images of ETS-10 crystals synthesized with molar formula of $5.56SiO_2$: $1.00TiO_2$: 1.67HCl: $2.69Na_2O$: 3.27NaCl: (n) KF, where n = 2.48 (a), 2.01 (b), 1.38 (c), 0.92 (d), 0.46 (e) and 0.09 (f) [41].

Figure 2.3 shows the summary of directions of the products. It indicates that the highest values for both *a* and *c* directions were obtained by minimizing the amount of KF in the reaction gel.

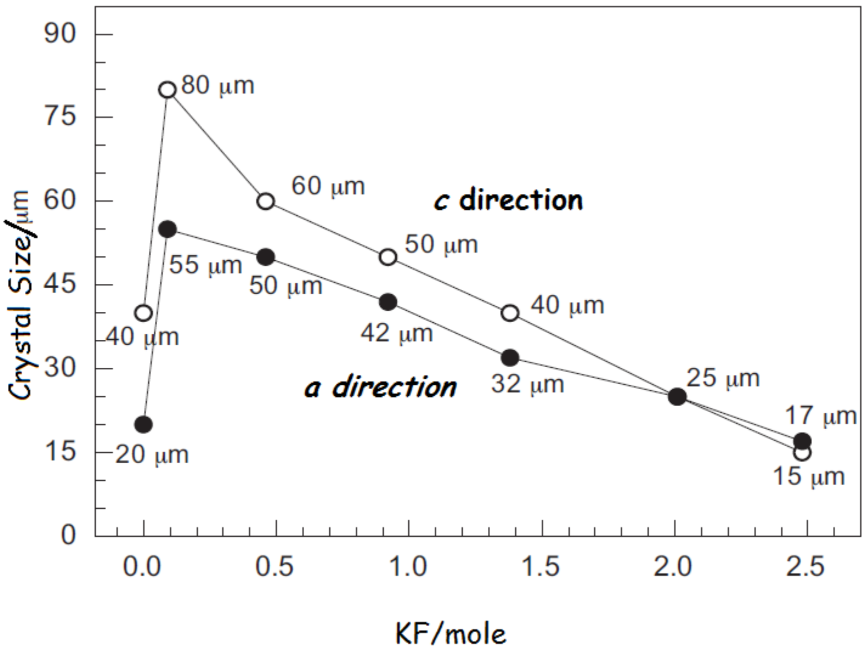

Figure 2.3. The summary of the directions of the products [41].

Depending on the application of synthesized ETS-10 crystals, it is reasonable to vary the water or KF amount in reaction gel. However, increasing water amount in the gel results in smooth crystals with the formation of unidentified impurity phase [40]. Consequently, altering KF in the gel seems to be more reasonable in order to control length of growth in the desired directions of ETS-10 crystals.

It is possible to obtain zeolite crystals having desirable size and morphology for numerous applications by managing the synthesis conditions. Moreover, controlling the inner structure; i.e. the size of micropores and/or the number of stacking defects in the zeolite framework is also critical for several applications of zeolites. This is not an easy task to accomplish, since zeolites have very rigid and well-defined pore structures. However, different post-treatment are applied frequently to make such changes into zeolite frameworks.

2.1.2 Post-treatment on Zeolite and Zeo-type materials

Managing the concentration and type of defects; i.e. stacking faults, line defects etc., is critical to enhance diffusion access through three dimensional pore system and catalytic activity [42]. An approach of defect formation is to alter synthesis parameter such as temperature and heating time, or adding structure directing agent during hydrothermal synthesis [43].

Moreover, several procedures such as usage of composite materials [44] and zeolite nanocrystals [45] or formation of intracrystalline mesoporosity [46] were applied to enhance the active sites or modify the pore size of zeolites. Intracrystalline mesoporosity could be achieved by post-synthesis treatment [47-53] It was described that dealumination caused during post-synthesis treatment through acidic medium provided partial mesoporosity in MFI type of zeolites and this post-synthesis treatment directly influenced acidic properties of treated zeolites [47]. Moreover, it was indicated that not only acidic treatment but also sodium hydroxide treatment of ZSM-5 type zeolites resulted in an increase in the total surface and external surface areas [48, 52].

It was stated that abundance of terrace nuclei on a growing surface leads to defect sites and increasing the rate of terrace nucleation with respect to terrace growth rate is critical to increase defects [53]. However, the crystallization process is not properly comprehended to control the concentration and type of the defects for ETS-10 [54]. Consequently, post synthesis treatment is more reasonable procedure to form defects inside ETS-10 crystals.

Only a few works has been performed as post synthesis treatment for ETS-10. Kromer et al. [55] displayed that ETS-10 exposed to citric acid exhibited appreciable activity in the alkene epoxydation. Llabréz i Xamena and coworkers [56] found that mild HF solution leads to silica leaching from the structure, enhancing the photocatalytic activity in degradation work of large aromatic molecules. Pavel and coworkers stated that different concentration and exposition time of hydrogen peroxide; i.e. H_2O_2, introduced different types of defects as well as stacking faults that formed during crystal synthesis [54]. Rearranged microporosity was observed after H_2O_2 treatment as seen in Figure 2.4.

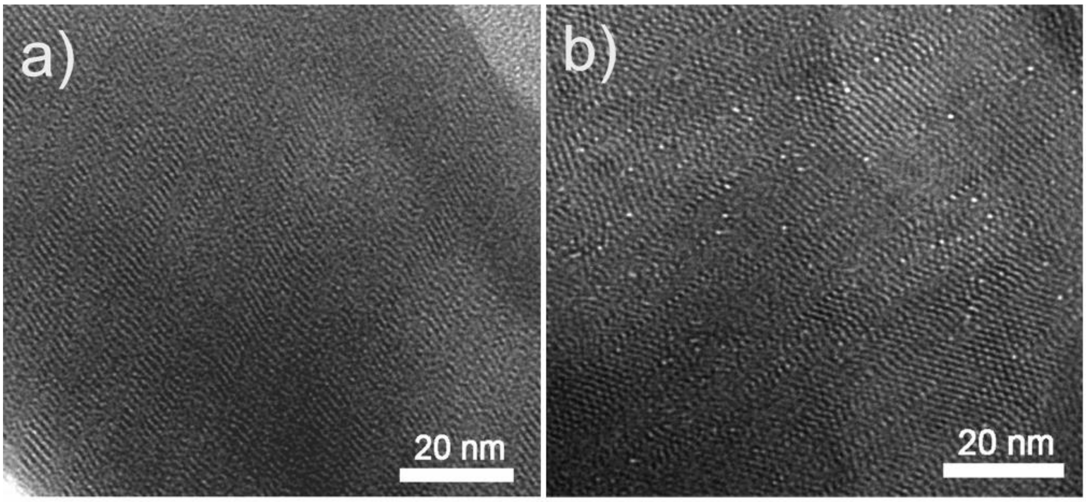

Figure 2.4. HR-TEM images of as-synthesized ETS-10 (a) and post-treated ETS-10 (b) [55].

H_2O_2 treatment to ETS-10 crystals can be a better post-treatment in order to introduce defects in crystal structure. Figure 2.5 shows schematic representation of partial Ti leaching and so Si leaching of ETS-10 crystal structure, forming defects inside ETS-10 crystals as Pavel *et. al* [54] described.

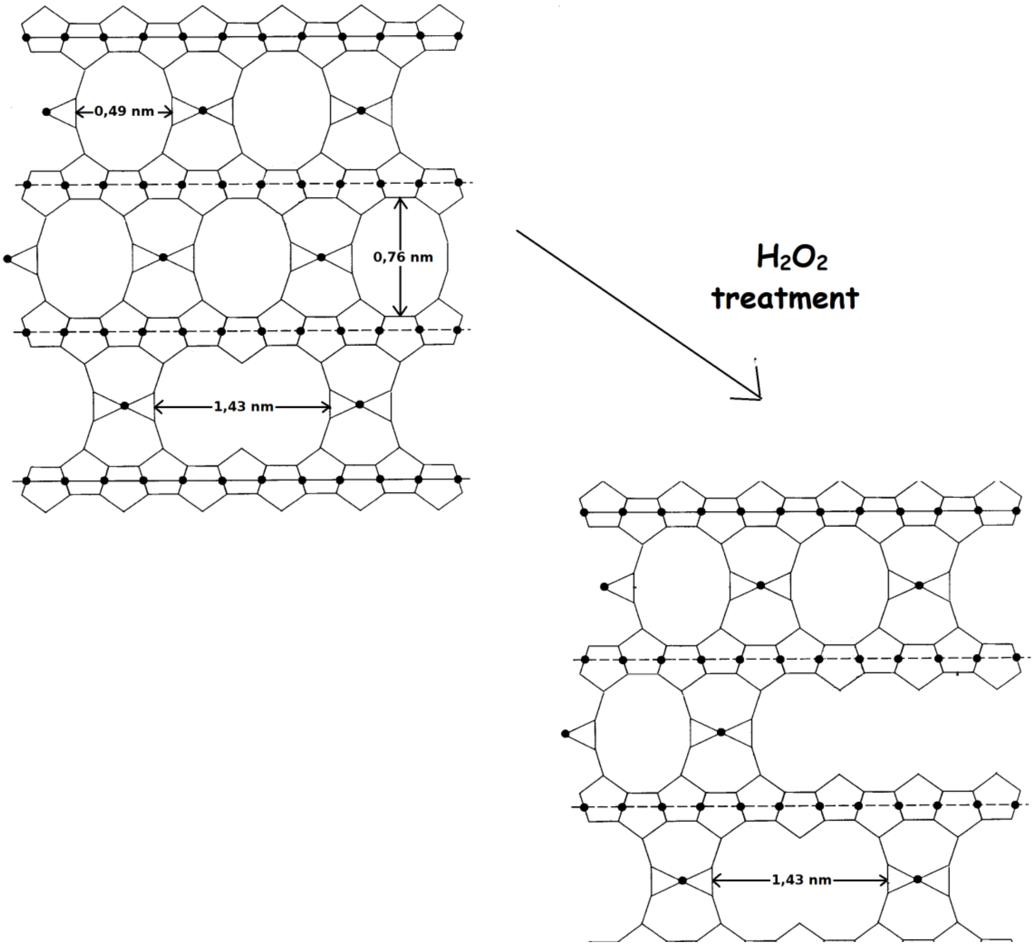

Figure 2.5. Schematic representation of the effect H_2O_2 and H_2SO_4 treatments on N-ETS-10 (Adapted from [6]).

2.2 Zeolites as host materials

The encapsulation of metal nanoparticles and metal complexes into zeolite framework sites has attracted great attention for many applications. Thus, numerous researches were performed about host-guest assembly for two decades.

2.2.1 Metallic Nanoparticles as guest for host-guest system

Novel metal nanoparticles such as silver were extensively studied in catalytic applications [8, 10]. It was stated that encapsulation of nanoparticles into zeolite framework enhanced the catalytic activity [8, 57-58].

Faroldi *et.al*. [59] reported that ruthenium nanoparticles incorporated into ETS-10 crystals was performed for hydrogen production. It was discussed that the effect of performing different method for nanoparticles incorporation into zeolite. Figure 2.6 and Figure 2.7 shows TEM images of ruthenium nanoparticles formation with different methods. As seen Figure 2.6, it was stated that nanoparticles produced by impregnation of ruthenium cations and reduction of these cations were well dispersed (Figure 2.6-a). However, after reduction of ruthenium cations added to ETS-10 synthesis gel in-situ, nanoparticles form clusters at the edges of the crystals, which could not be observed any dispersion on crystals (Figure 2.6-b).

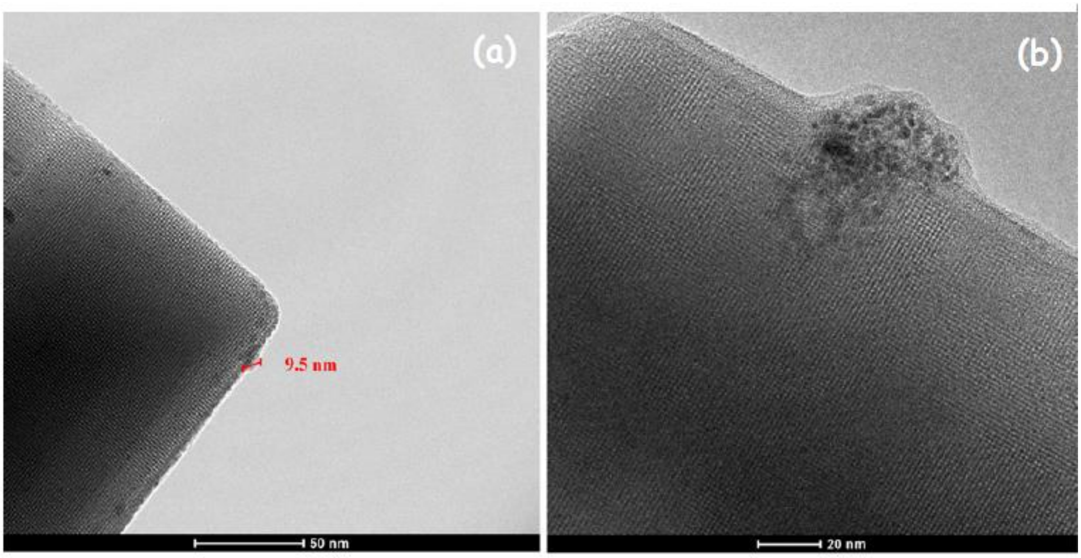

Figure 2.6. TEM images of after chemical reduction of ruthenium cations impregnated ETS-10 (a) and ruthenium cations added synthesis gel (b) [59].

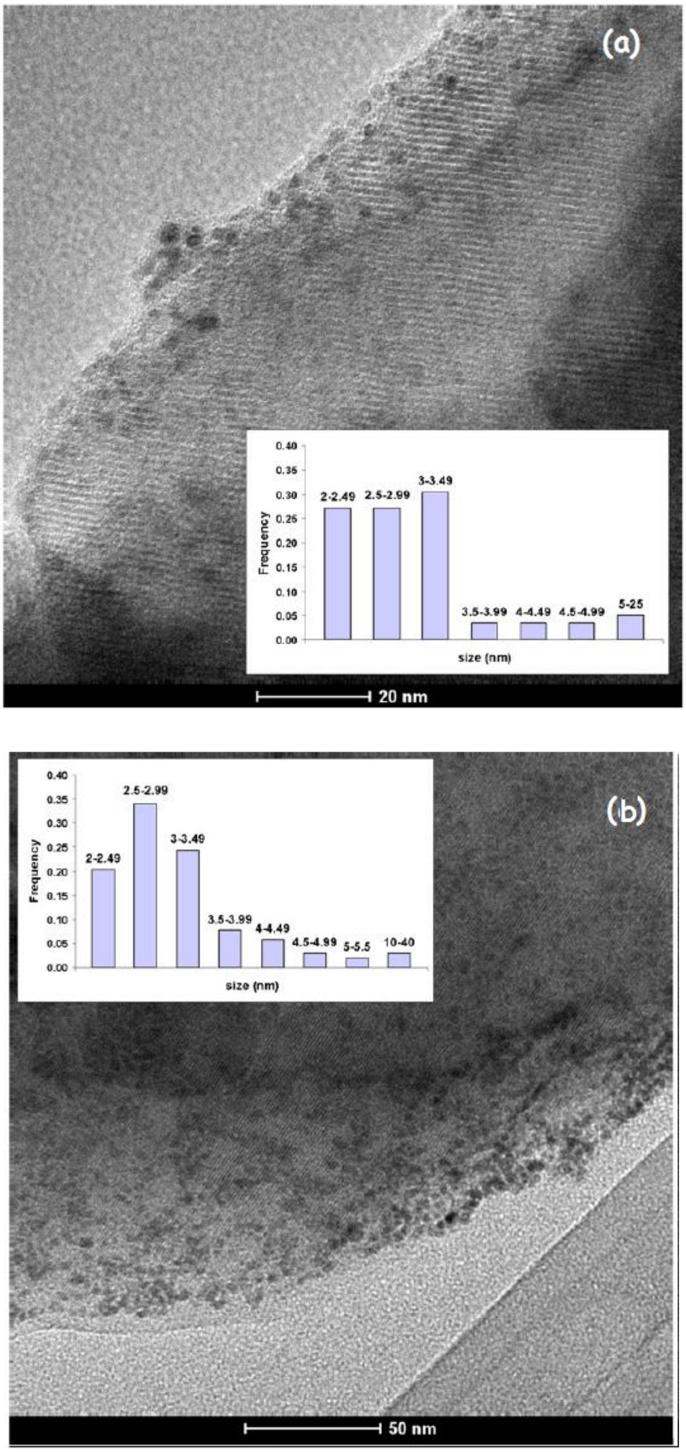

Figure 2.7. TEM images of samples formed by ion-exchange with low (a) and high (b) concentration of ruthenium cations [59].

Moreover, Figure 2.7 shows that the effect of concentration of ruthenium cation in ion-exchange of ETS-10 crystals. It was reported that the size of ruthenium nanoparticles formed was generally in the range of 2-3.5 nm from EDX results and there was no obvious effect of ruthenium concentration at synthesis gel on the size of nanoparticles formed [59].

2.2.2 Dyes as guest for host-guest system

Not only nanoparticles but also dye molecules are preferred as guest molecules for host-guest systems. There are four approaches to incorporate dyes into porous materials; ship-in-a-bottle synthesis [60], loading of cationic dyes [61], vapor phase deposition [62] and crystallization encapsulation [63]. In this thesis, first two were covered and discussed in Chapters 3 and 4.

2.2.2.1 Ship-in-a-bottle synthesis of dye molecules in Zeolite Matrix

Zeolites are microporous crystals possessing large holes organized with smaller windows. Although, guest molecules have a suitable size to accommodate into the zeolite cages, it may not be possible for these guest molecules to diffuse through zeolite windows due to the smaller opening sizes of windows with respect to the molecules. Consequently, ship-in-a-bottle synthesis can be an alternative and desirable approach to form the guest molecules in zeolite cages. During the ship-in-a-bottle approach, reactants are introduced through the windows and thus the desired guest products are formed inside the host. Ship-in-a-bottle synthesis is often preferred by using zeolite X and Y as host compounds due to the large interior cage that these zeolite types possess.

Xu *et. al*. [64] reported that Ir(III) complexes were formed in the zeolite X cages through ship-in-a-bottle synthesis. Three different pyridine ligands were used in the synthesis one by one to form organometallic dye molecules in zeolite X matrix. Figure 2.8 shows the representation of the synthesis. Ion-exchange was performed to introduce Ir(III) cations in the framework and complexes were synthesized by addition of ligands in the reaction systems. To carry out the synthesis of Ir(III) complexes, microwave irradiation was used.

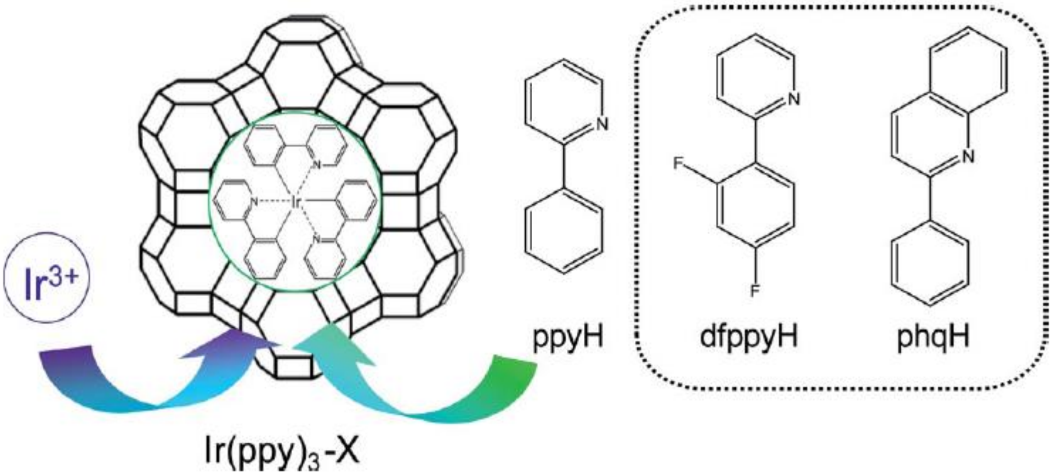

Figure 2.8. Synthesis of Ir(III) complexes with three different ligands in the supercages or on the surface of zeolite X [64].

The fluorescence and absorbance properties of the resulting encapsulated Ir(III) complexes by zeolite X were compared with each other. It was stated that washing with toluene caused removal of the complex formed on surface of zeolite. After washing with toluene, the emission spectrum of $[Ir(phq)]^{3+}$ decreased, which indicated formation of complex on zeolite surface and not inside the zeolite. Xu *et. al* explained this result with the size of $[Ir(phq)]^{3+}$that is known to be 1.3 nm, which is equal to the size of zeolite X supercage, whereas the sizes of others are smaller.

Another study about ship-in-a-bottle synthesis is synthesis of tris(2,2'-bipyridine)ruthenium(II); i.e. $[Ru(bpy)_3]^{2+}$, complexes within zeolite Y [61]. In this research, zeolite Y was exchanged with $[Ru(NH)_6]^{2+}$ cations. After ion-exchange resulting product was introduced with 2,2'-bipyridine to form $[Ru(bpy)_3]^{2+}$. Dewilde *et.al.* [61] stated that zeolite lattice did not considerably influence the relative energy between metal ion and the ligands.

Laine *et al*. [65] reported that ship-in-a-bottle synthesis of $[Ru(bpy)_3]^{2+}$ in the zeolite Y matrix was successfully achieved in the cavities of zeolite Y. Performing several chemically consecutive destructive and nondestructive methods, the concentration of $[Ru(bpy)_3]^{2+}$ on the surface of zeolite Y crystals and inside zeolite Y crystals were determined. It was shown that up to 50% of dye products were placed in the pores, which is $[Ru(bpy)_3{}^{2+}]_{core}$ in expression;

$$[Ru(bpy)_3{}^{2+}] = [Ru(bpy)_3{}^{2+}]_S + [Ru(bpy)_3{}^{2+}]_{core} \qquad (2.1)$$

$$\Theta_S = \frac{[Ru(bpy)_3{}^{2+}]_S}{[Ru(bpy)_3{}^{2+}]} \text{ x } 100 \qquad (2.2)$$

where $[Ru(bpy)_3{}^{2+}]$ is the total number of $[Ru(bpy)_3]^{2+}$ molecules synthesized, $[Ru(bpy)_3{}^{2+}]_S$ is the number of $[Ru(bpy)_3]^{2+}$ molecules synthesized on surface of crystals and Θ_s is the distribution parameter of $[Ru(bpy)_3]^{2+}$ synthesized on surface of crystals. Also, distribution paramater of $[Ru(bpy)_3]^{2+}$ on the surface of zeolite Y is denoted as Θ_s.

Laine and coworkers reported that it was obtained $[Ru(bpy)_3]^{2+}$ in supercages of zeolite Y up to about 65% when using the zeolites, which in dye was formed previously, during ion-exchange procedure According to Laine *et. al.*, Figure 2.9 shows that saturation of zeolite pores with dye resulted in a sharp increase in Θ_s.

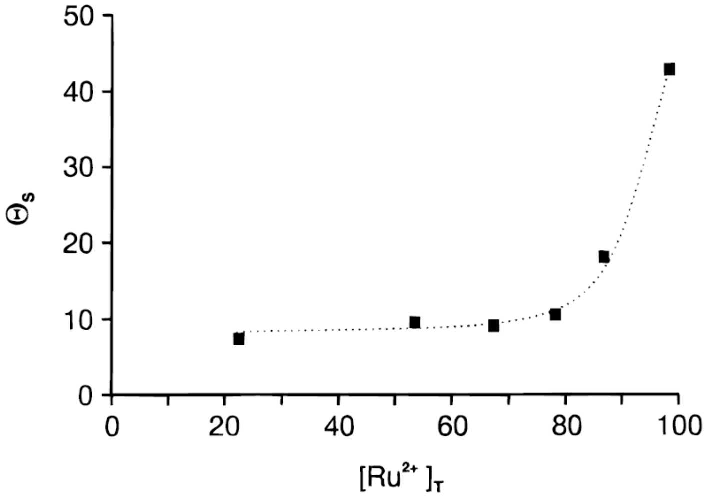

Figure 2.9. Distribution parameter of $[Ru(bpy)_3]^{2+}$ on the surface of zeolite Y; i.e. Θ_S depending on total ruthenium content of the system produced from previously dye formed samples [65].

2.2.2.2 Loading Dye molecules to Zeolites

Dye incorporation into zeolites can be applied also by loading the dye if the size of dye molecule is suitable to diffuse the channel/cavities of zeolites. Loading dye molecules into zeo-type structures is an alternative method to form a microlaser [66-69]. It was indicated that rhodamine 6G dye, was loaded into mesoporous titania [69], showing advanced laser emission possessions. This nanocomposite can be used in any application of optically active devices due to its property of easy fabrication with lithography [69].

Furthermore, one of the instances of loaded dye molecules into zeolites is that $AlPO_4$-5, a zeo-type material possessing 1-D channel, as host and 2,2'-bipyridine-3,3'-diol dye as guest as seen in Figure 2.10. Rurack et al. [70] directly mixed 2,2'-bipyridine-3,3'-diol solution and $AlPO_4$-5, in which dye molecules diffused through channels of zeo-type material by means of solvent, and vaporized this solvent after insertion. The resulting composite is dye molecules attached to zeo-type material. It was observed that the host-guest assembly possesses strong fluorescence and the resulting material showed optical anisotropy, which indicated that dye molecules were placed into the $AlPO_4$-5 uniformly [70].

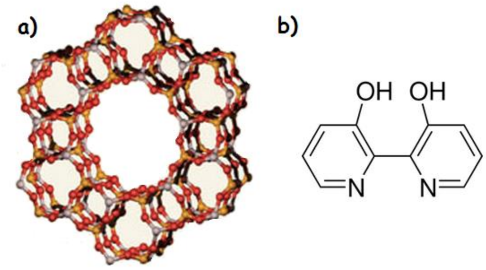

Figure 2.10. The structure of $AlPO_4$-5 possessing 1-D channels, adapted from [71] (a) and 2,2’-bipyridine-3,3’-diol (b).

More than one type of dye molecules could be loaded into pores/channels of zeolites or zeo-type materials as guest through special designs as well. Calzaferri and his coworkers stated that multi-component dyes display remarkable energy-transfer systems, which are named as zeolite antenna [27, 72-74]. It was reported that encapsulation of pyronine and oxinine molecules; cationic dyes, in zeolite L was an attractive assembly for light harvesting systems [27]. Figure 2.11 shows that emission wavelengths of pyronine; i.e. 470-490 nm, and oxinine; i.e. 545-580 nm, are different as well as fluorescence microscopy images.

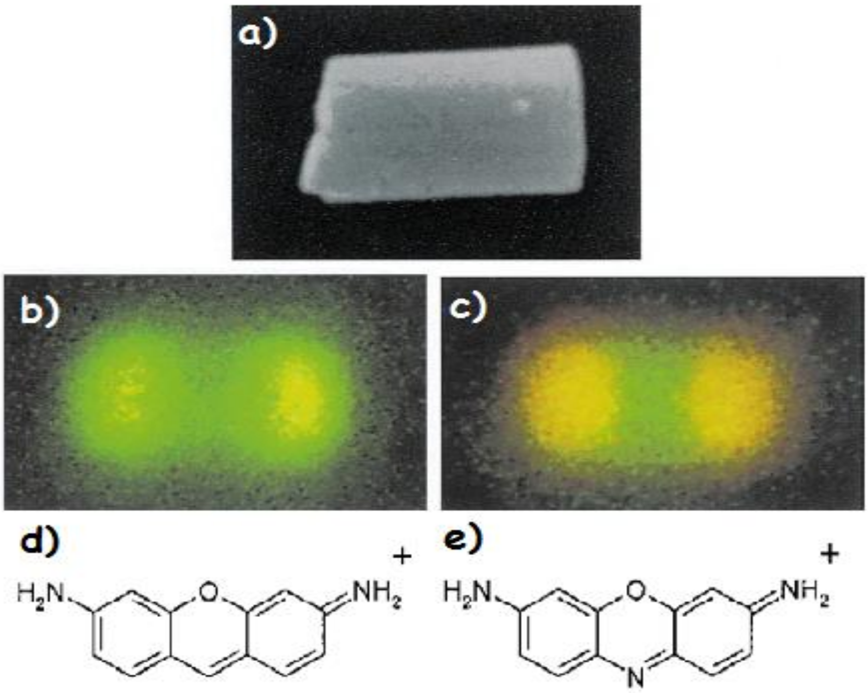

Figure 2.11 SEM image of a zeolite L crystal with a length of 1500 nm (a), fluorescence microscope images of 2 h exchange with pyronine (b), after additional 2 h exchange with oxonine (c), and the chemical structures of pyronine (c) and oxinine (d) [27].

An external energy is absorbed by zeolite L crystals, and this energy is transferred to pyronine and oxinine, respectively in this host-guest system designed by Calzaferri *et al.* [27]. Figure 2.12 is the schematic representation of the summary of energy harvesting procedure. In combination of guests, pyronine molecule acted as donor and oxinine acted as accepter in electron transfer inside zeolite. In this figure, white rectangles represented pyronine molecules (Py^+) aligned though zeolite L channels, whereas black rectangles represented oxinine molecules (Ox^+). Furthermore, the arrow showed the direction of energy transfer, in which k_F showed the rate of fluorescence of corresponding dyes, k_{EM} is the rate constant of energy transfer and k_{ET} is the rate constant of energy transfer from pyronine to oxinine molecules. Combining two different dye molecules provides larger rate constant of fluorescence, which leads to an increase in the efficiency of energy migration.

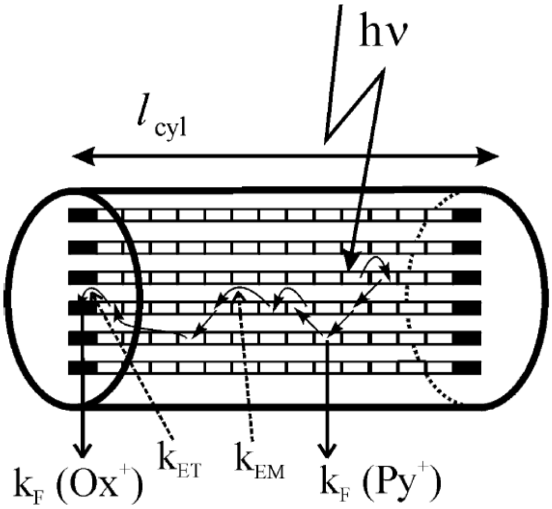

Figure 2.12. A schematic representation of antenna designed with pyronine, oxinine dyes and zeolite L [74].

CHAPTER 3

EXPERIMENTAL

3.1 General

To investigate ETS-10 as a host material, the first objective was to synthesize ETS-10 with desired size and morphology. ETS-10 crystals were subsequently modified through post-synthesis treatment to enlarge micropores of ETS-10. Additionally, the inclusion of metallic nanoparticles and organometallic dye molecules were carried out within the ETS-10.

Sodium silicate (Na_2SiO_3, 17–19% Na_2O, and 35–38% SiO_2, Kanto), titanium isopropoxide [Ti(*i*PrO)4, 98%, Junsei], hydrochloric acid (HCl, 35–37%, Samchun), sodium chloride (NaCl, 99%, Samchun), and potassium fluoride (KF, 98%, Samchun) were purchased and used without further purification.

The chemicals; TiO_2 (P25, 76 wt. % anatase and 24 wt. % rutile, Degussa), $NaSiO_2$, $RuCl_3.H_2O$, $[Ru(NH)_3]_6Cl_2$, 2’2,-bipyridyl, pyronine, H_2O_2 (wt. %50 in H_2O), $NaBH_4$ and LUDOX (HS-40 col. Silica 40% in H_2O) were obtained from Sigma-Aldrich. NaCl (99.0%), KCl (99.0%), and H_2SO_4 (96.5%) were received from J.T. Baker. $Al_2[(SO)_4]_3.16H_2O$ was procured from Fluka.

3.2 Synthesis of ETS-10

3.2.1 Synthesis of M-ETS-10

M-ETS-10 crystals; possessing size with larger than 1 μm, were obtained from the gel formula; $5.56SiO_2$: TiO_2: xHCl: $2.69Na_2O$: 3.27NaCl: yKF: $219H_2O$, where x=1.67, 1.99 and y=2.01, 0.92 and 0.09 [41].The gel were obtained as follows; Si precursor was prepared by diluting 45.71 g sodium silicate solution with 50.41 g deionized water. The aqueous solution of sodium chloride, that was prepared previously with 9.13 g sodium chloride and 30.20 g deionized water, was added into the silicate solution and stirred vigorously for 2 hours. Ti precursor was prepared in another bottle through adding 10.32 g titanium isopropoxide into aqueous hydrochloric acid solution and stirred for 2 hours at room temperature. The clear Ti solution was added into Si solution in a drop wise manner. Then, the mixture was stirred for 1 hour at room temperature. An aqueous KF solution was added into Si-Ti solution that was prepared previously. The mixture was aged for 16 hours at room temperature and placed into 10 mL Teflon-lined stainless steel autoclaves. The static syntheses were performed for 4 days at 503 K. Products were cooled at room temperature, washed with deionized water, collected through centrifugation, and dried for one day at 323 K.

3.2.2 Synthesis of N-ETS-10

N-ETS-10 crystals were synthesized using the gel composition 3.4 Na_2O: 1.5 K_2O: TiO_2: 5.5 SiO_2: 150 H_2O [76]. For the synthesis, 1.62 g sodium chloride and 2.48 g potassium chloride were dissolved in 14.14 g deionized water. 13.09 g sodium silicate was added into the aqueous salt solution in a high density polyethylene bottle (HDPE) and hand-shaken for 5 min, forming the Si precursor solution. For the formation of Ti source, 0.88 g commercial TiO_2 (P25) was added into an aqueous solution of sulfuric acid solution prepared by mixing 0.75 g sulfuric acid with 7.07 g deionized water. The solution was hand-shaken vigorously for 5 min. The resulting white, viscous solution was obtained by pouring the Ti precursor solution into the Si precursor solution and hand-shaken for 5 min. After measuring the pH of the solution (pH =10.6-10.8) using an Hanna 2211 pH/ORP meter, the gel was introduced into 10 mL Teflon-lined stainless steel autoclaves for 72 hour at 503 K. After synthesis, the crystals were cooled at room temperature, centrifuged and washed with deionized water several times and lastly dried for a day at 323 K.

3.2.2.1 Modification of Crystal Structure of N-ETS-10 with Hydrogen peroxide and Sulfuric acid

Hydrogen peroxide (H_2O_2) treatment was applied in order to create defects in N-ETS-10, which was hypothesized to break the framework bonds and increase the micropore volume. For this purpose, two different set of samples were prepared according to Pavel *et al*. [54] as shown in Table 3.1. In the first set, original N-ETS-10 sample was subjected to a one-shot H_2O_2 treatment of 30 wt. % H_2O_2 for 30 minutes at room temperature. The samples are denoted as N-ETS-10-30%(1), where 30% represents H_2O_2 with concentration of 30wt. % and (1) represents the number of consecutive H_2O_2 treatment. After H_2O_2 treatment, crystals were washed, centrifuged several times and dried at 323 K for one day.

In the second set of samples, three consecutive H_2O_2 treatment of 10 wt. % were performed where each treatment was applied for 20 minutes. The sample are denoted as N-ETS-10-10%(3), where 10% represents H_2O_2 with concentration of 10wt. % and (3) represents the number of consecutive H_2O_2 treatment. The crystals were washed, centrifuged several times and dried at 323 K for one day.

After H_2O_2 treatment, ETS-10 crystals were subjected to further sulfuric acid (H_2SO_4) treatment in order to prevent crystals from potential stacking of disposal side products (i.e., $Ti(OH)_4$ and $Si(OH)_4$). 0.2 g of N-ETS-10-30%(1) and N-ETS-10-10%(3) were added into 5 mL of 1M aqueous H_2SO_4 solution for 4 hour [76, 77]. The treated ETS-10 crystals were washed with deionized water several times, centrifuged and dried at 323 K for a day. The modified crystals were denoted as N-ETS-10-30%(1)-S and N-ETS-10-10%(3)-S for N-ETS-10-30%(1) and N-ETS-10-10%(3), respectively.

Table 3.1. The summary of post-synthesis treatments with H_2O_2 and H_2SO_4 conditions.

System Code	H_2O_2 Concentration (wt. %)	H_2O_2 Contact Time (min)	H_2SO_4 Concentration (M)	H_2SO_4 Contact Time (hour)
N-ETS-10-30%(1)	30%	30	–	–
N-ETS-10-30%(1)-S	30%	30	1	4
N-ETS-10-10%(3)	10% x3 (3 times with fresh 10% solution)	20 (for every treatment)	–	–
N-ETS-10-10%(3)-S	10% x3 (3 times with fresh 10% solution)	20 (for every treatment)	1	4

The samples were all subjected to further analysis to determine the changes induced into the framework structure. Afterwards, the metallic nanoparticle formation was investigated in these samples to observe change in the particle size distributions.

3.3 ETS-10 as a host material

The novel approach of this study is that a host-guest assembly was tried to be prepared, in which ETS-10 is as host material, whereas ruthenium nanoparticles *(i)* or tris(2,2′-bipyridyl)ruthenium(II), dye molecule, *(ii)* is the guest. Ruthenium nanoparticles were formed incorporation into ETS-10 having size with 500-600 nm; i.e. N-ETS-10. However, ship-in-a-bottle syntheses of tris(2,2′-bipyridyl)ruthenium(II) in ETS-10 were applied in larger size ETS-10; i.e. M-ETS-10.

3.3.1 Preparation of Ruthenium Nanoparticles incorporated into N-ETS-10 crystals

Ru^0 nanoparticles incorporated ETS-10 crystals were formed by two sequential steps. Firstly, exchangeable extra framework cations (i.e., Na^+ and K^+) in N-ETS-10 were exchanged with Ru^{3+} ions by using different concentration of ruthenium(III) chloride solution. Aqueous sodium borohydride solution was used to reduce Ru^{3+} ions to Ru^0 nanoparticles at room temperature.

3.3.1.1 Ion-exchange and Reduction of Ru^{3+} Ions

In order to obtain Ru^{3+}-exchanged ETS-10 crystals, 0.137 g $RuCl_3.nH_2O$ 4 was added into 100 ml of 500 mg as-synthesized N-ETS-10 suspension. The solution was mixed vigorously for 72 hours at room temperature. After ion-exchange, the samples were washed and centrifuged. Ruthenium nanoparticles incorporated into N-ETS-10 was obtained by reducing Ru^{3+}-exchanged N-ETS-10 in sodium borohydride ($NaBH_4$) suspension at room temperature. The reaction represent as;

$$NaBH_4 + 2H_2O \rightarrow NaBO_4 + H_2 \tag{3.1}$$

Ruthenium nanoparticles, stabilized by zeolite framework, were formed. Observing H_2 outflow by naked eye is the evidence that chemical reduction has been applied successfully. The samples were washed with 1 L of deionized water and centrifuged after reduction was complete and then they dried overnight at 273 K.

3.3.2 Preparation of dye molecules incorporated into ETS-10 crystals

Tris(2,2′-bipyridyl)ruthenium(II) cationic dye molecules were synthesized in M-ETS-10 matrix. The synthesis consists of two steps; first one is ion exchange extra-framework cations; i.e. Na, K with ruthenium atoms in ETS-10 framework and second one is the reaction of ruthenium and 2,2′-bipyridyl the in the ETS-10 matrix. This type of synthesis is named as “ship-in-a-bottle synthesis”. In the literature, ship-in-a-bottle syntheses of tris(2,2′-bipyridyl)ruthenium(II) cationic dye molecules incorporated into zeolite Y were applied [31-36]. In this study, not only cationic dye synthesis in ETS-10 matrix, but also in zeolite Y matrix was performed. Zeolite Y, which was already synthesized in our group [78], was used for the synthesis.

Furthermore, there are some studies about loading of dye molecules into zeolite framework. Calzaferri has many publications about pyronine loaded zeolite L host-guest systems [27, 79-81]. Moreover, in order to discuss and compare ship-in-a-bottle synthesis and loading of dye molecules into ETS-10 framework, commercial pyronine was purchased and loaded into ETS-10.

3.3.2.1 Tris(2,2'-bipyridyl)ruthenium(II) cation incorporated into ETS-10

Two basic steps were followed to synthesize tris(2,2'-bipyridyl)ruthenium(II) cation in ETS-10 matrix; namely, (i) ion exchange sodium ions with ruthenium ions by using two different ruthenium source chemicals, ruthenium(III) chloride hydrate; i.e. $RuCl_3.nH_2O$*, and hexaamineruthenium chloride; i.e.* $[Ru(NH)_6]Cl_3$*, (ii) reaction of ruthenium ions with 2,2'-bipyridyl molecules in ETS-10 matrix. The summary of reaction equations are represented as;*

$$\begin{tikzcd}
 & {[Ru(NH)_6]^{3+} - ETS - 10} \quad \text{(RuNH-M-ETS-10)} \\
Na^{+} - K^{+} - ETS - 10 \arrow[r, "ion\ exchange"] & \textbf{or} \\
 & Ru^{3+} - ETS - 10 \quad \text{(Ru-M-ETS-10)} \arrow[dl, "in\ reflux"] \\
{[Ru(bpy)_3]^{2+} - ETS - 10} &
\end{tikzcd}$$

(3.2)

In the ruthenium ion-exchange step, 0.237 g $[Ru(NH)_6]Cl_3$, was added into 100 ml of 600 mg M-ETS-10 suspension using $[Ru(NH)_6]Cl_3$ as a ruthenium source. Color of resulting mixture was light grey. The synthesis in which used $[Ru(NH)_6]Cl_3$ is denoted as RuNH-M-ETS-10. However, 0.176 g $RuCl_3.nH_2O$ was added into 100 ml of 500 mg M-ETS-10 suspension when using $RuCl_3.nH_2O$

as ruthenium source. Hydrate number “n” in one mole of $RuCl_3$ calculated in previous study [82], which is 3, was used. Color of resulting mixture was black. The synthesis in which used the other ruthenium source; i.e. $RuCl_3.nH_2O$, was denoted as Ru-M-ETS-10 as summarized in Table 3.2. Ruthenium ion exchanged crystals were washed with deionized water, centrifuged and dried at 323 K for one day.

Table 3.2. The summary of the reactants for RuNH-M-ETS-10 and
Ru-M-ETS-10.

System Code	Reagent-I	Reagent-II
RuNH-M-ETS-10	$[Ru(NH)_6]Cl_3$	2,2’-bipyridyl
Ru-M-ETS-10-10	$RuCl_3.nH_2O$	2,2’-bipyridyl

In the second step the synthesis of organometallic complex within ETS-10 matrix was achieved. In-situ synthesis of tris(2,2′-bipyridyl)ruthenium(II) cation within ETS-10 matrix was carried out in a reflux system as seen in Figure 3.1. The powder ruthenium source and stir bar were placed into two-neck round-bottom flask. To remove humidity inside the flask, a balloon, full with inert Argon gas, was connected to top of the reflux system. After almost six hours evacuation, 2,2′-bipyridyl dissolved in 40 mL isopropyl alcohol, was added into flask with syringe. The reaction solution was stirred at room temperature for 4 hours, afterwards at 200 ^{0}C for 24 hours [61]. The colors of solutions after centrifuged with deionized water three times were pinkish-purple for RuNH-M-ETS-10 as reported in literature [31] and black for Ru-M-ETS-10.

Also, the same procedure of the synthesis of tris(2,2′-bipyridyl)ruthenium(II) cation incorporated ETS-10 was used to synthesize of incorporated zeolite Y instead of ETS-10 as ship-in-a-bottle synthesis. Zeolite Y used for this synthesis was already synthesized in our group [78].

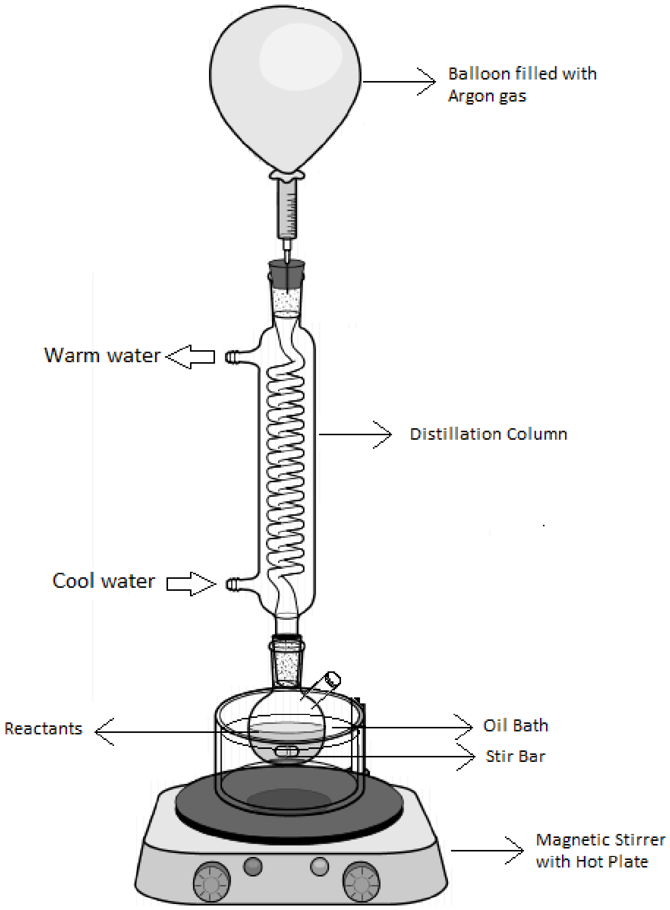

Figure 3. 1. A schematic representation of the reflux system used for the synthesis of tris(2,2′-bipyridyl)ruthenium(II) cation incorporated ETS-10.

3.3.3 Loading cationic dyes to Zeolites/Zeo-type Material

Commercial pyronine was loaded into M-ETS-10 as another procedure for dye incorporated into zeolite. 80 mg M-ETS-10 was added to 40 mL of $1x10^{-6}$ M aqueous pyronine solution. The resulting solution was sonicated for 10 minutes and later transferred into two-necked round bottom flask to boil at reflux at 100 °C for 2 hours. After reflux, the mixture was centrifuged and dried at room temperature in vacuum [83].

3.4 Material Characterization

3.4.1 X-Ray Diffraction (XRD)

The powder X-Ray diffraction studies were carried out using a Rigaku Ultima IV X-Ray diffraction at METU Central Laboratory. Bragg-Brentano diffractometer monochromated Cu Kα radiation and equipped with curved graphite crystal diffracted beam monochromator and a NaI scintillation detector was used. The X-ray beam was operated at 30 mA and 40 kV. The range of collected data is between 5-40° 2ϴ degrees with step size of 1 °/min and the slit was 0.2 mm and time was constant as 1 s.

3.4.2 Scanning Electron Microscopy (SEM)

The field emission scanning microscopy was performed to characterize the morphology of powder as-synthesized and nanoparticle incorporated ETS-10 crystals using a QUANTA 400F Field Emission SEM in the secondary electron imaging mode at METU Central Laboratory. Small amount of crystals were dissolved in deionized water, dropped into aluminum sample holder coated with carbon paint and evaporated. Each sample was analyzed several times to ensure the reliability of data.

3.4.3 Inductively Coupled Plasma – Mass Spectrophotometer (ICP-MS)

Sodium, potassium, silicon and titanium content were determined before and after H_2O_2 and H_2SO_4 treatments by inductively coupled plasma mass spectrometry (ICP-MS) (Thermo Scientific X Series II) at National Nanotechnology Research

Center in İhsan Doğramacı Bilkent University. And also ICP-MS was performed to detect the content of ruthenium content of the ion-exchanged and ETS-10 containing ruthenium nanoparticle after total dissolution of the ETS-10 samples.

3.4.4 UV-VIS Spectroscopy

The UV-visible spectra in diffuse reflectance mode were recorded with solid samples on a Shimadzu (UV-2450) UV-VIS spectrophotometer at Department of Chemistry at METU. The range was from 200 to 800 nm. The solid samples were prepared by mixing barium sulfate ($BaSO_4$)) and pressing this mixture to form pellets. The recorded diffuse reflectance spectra were converted into absorbance spectra with respect to Kubelka Munk function, which is;

$$f(A) = \frac{(1-R)^2}{2 \times R} \tag{3.1}$$

where R is recorded diffuse reflectance, $f(A)$ is relative absorbance of samples.

3.4.5 Surface Area and Pore Size Distribution Analysis

Surface area and pore size distribution analysis were performed for the samples before and after ruthenium incorporation and post-treated samples in order to determine the difference in pore size and surface areas. The nitrogen adsorption and desorption isotherms were carried out by Quantachrome Corporation Autosorb-6B instrument in METU Central Laboratory.

3.4.6 Transmission Electron Microscopy (TEM)

Transmission electron microscopy was carried out to indicate the morphological difference in the samples of as-synthesized, post-treated, and ruthenium nanoparticle incorporated ETS-10 crystals. Small amount of ETS-10 ethanol suspension dropped into copper grid was used at JEM-2010F microscope (JEOL) at METU Central Laboratory. 200 kV of operating voltage was for TEM imaging.

3.4.7 Fourier Transform Infrared Spectroscopy (FT-IR)

For the analyses of characteristic vibration bands of m-ETS-10 with and without incorporation of dye molecules, Fourier Transform infrared spectra were acquired at Bruker IFS/66S at METU Central Laboratory. Potassium bromide was used as the background and powder samples were analyzed neat.

3.4.8 Raman Spectroscopy

Raman Spectroscopy analyses were performed to indicate the characteristic bands of N-ETS-10 and N-ETS-10 incorporated ruthenium nanoparticles at Ramanscope II de Raman Spectroscopy in METU Central Laboratory. For the analyses, 1064 nm Nd-YAG laser was used.

3.4.9 Epi-fluorescence Microscopy (EFM) and Confocal Laser Scanning Microscopy (CLSM)

Zeiss LSM 510 was used for transmitted light, widefield fluorescence and confocal laser scanning images of $[Ru(bpy)_3]^{2+}$ and pyronine, which have high emission in visible and UV range after excitation. HBO lamp was used as source to obtain widefield fluorescence image and laser source was used for confocal laser scanning images. 40x and 100x objectives were used to obtain high quality images. The samples dissolved in ethanol were treated sonication. The solutions were dropped into glass slide and covered with lamellae in order to prevent solvent evaporation before they were placed into microscopy. Both $[Ru(bpy)_3]^{2+}$ and pyronine cations were excited at 477 nm, emissions were collected in range between 500-800 nm. The analyses were performed at METU Central Laboratory.

CHAPTER 4

RESULTS AND DISCUSSION

4.1 Synthesis of M-ETS-10

The synthesis of relatively large ETS-10 crystals with particle size in several micometer region (M-ETS-10) has been a challenge. For that purpose, M-ETS-10 crystals were synthesized using the molar formula of 5.56SiO2: TiO2: xHCl: 2.69Na2O: 3.27NaCl: yKF: 219H2O, where x=1.67, 1.99 and y=2.01, 0.92 and 0.09 [41]. Table 4.1 indicates the summary of the reaction gel composition with different molar concentrations of HCl and KF and their effects on the size of the crystals.

To clarify the importance of fluoride amount in the reaction gel where HCl was 1.99, the amount of KF in the synthesis gel was varied with the molar formula of $5.56SiO_2$: TiO_2: 1.99HCl: $2.69Na_2O$: 3.27NaCl: yKF: $219H_2O$, where y=0.09, 0.92 and 2.01. The samples were denoted as S1 for y=0.09, S2 for y=0.92 and S3 for y=2.01.

Table 4.1 Summary of the effect of molar concentrations of HCl and KF on reaction gel for the synthesis of M-ETS-10.

System Code	*x* (HCl)	*y* (KF)	Crystallinity	Size (µm)
S1	1.99	0.09	Amorphous	_
S2	1.99	0.92	Crystalline	a=36.4, b=29.9, c=32.9
S3	1.99	2.01	Crystalline	a=44.8, b=44.9, c=18.4
S4	1.67	0.09	Amorphous	_
S5	1.67	0.92	Crystalline	a=50.6, b=49.5, c=39.9
S6	1.67	2.01	Crystalline	a=49.1, b=44.3, c=18.3

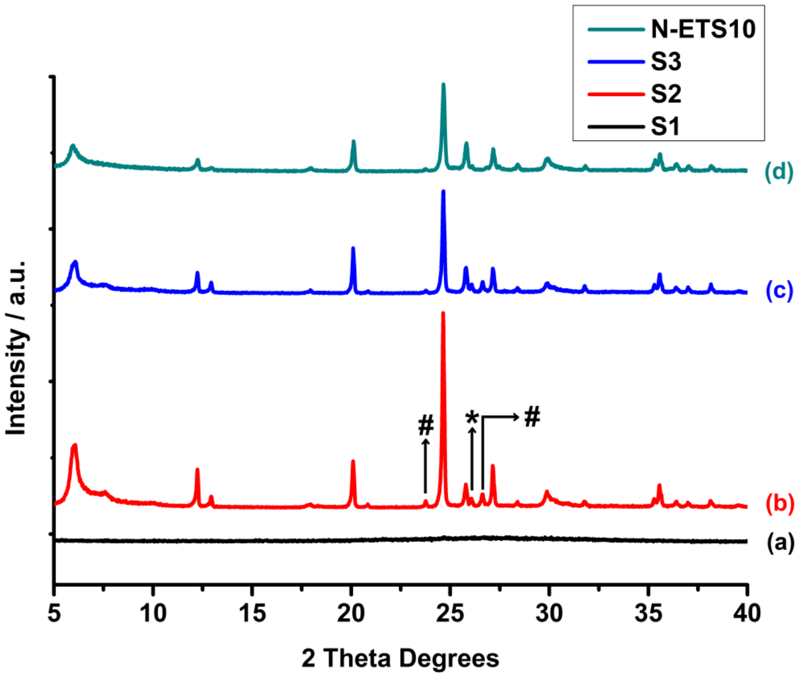

Figure 4.1. XRD patterns of M-ETS-10 (with 1.99 M HCl) with different KF molar ratio. KF molar ratios are 0.09 for S1 (a), 0.92 for S2 (b) 2.01 for S3 (c) and N-ETS-10 (d). * indicates AM-3 formation and # indicates quartz formation.

X-ray diffraction patterns of S1, S2 and S3 are shown in Figure 4.1. N-ETS-10 was used as reference ETS-10 sample and its details are discussed in Section 4.3. According to Figure 4.1, S1 has an amorphous structure. Furthermore SEM image of S1 as shown in Figure 4.1-a indicates that there are notable unreacted species in the sample in Figure 4.1-a due to lack of KF amount in gel.

Increasing KF amount to 0.92 M for sample S2 and 2.01 M for sample S3 resulted in an increase in the crystallinity of sample when compared to N-ETS-10 (Figure 4.1-b). However, it was observed that higher fluoride ion content caused an increase in quartz impurity formation in the final product. According to Rocha *et al.* [84], fluoride ions, having smaller ionic radius than hydroxyl groups, are capable of attacking Si atoms. And this attacking can cause polymerization of silicate species [84]. Therefore, fluoride content of reaction gel might lead to increase in quartz impurity. Moreover, S2 and S3 contain impurities due to reflection of AM-3 formation when comparing to N-ETS-10 (Figure 4.1) [20].

SEM images of S2 and S3 showed that crystals have uniform size and almost truncated bipyramid morphology (Figure 4.2). As the mole ratio of KF increases, *a* and *b* directions of the crystals elongated from 36.4 and 29.9 for S2 to 44.8 and 44.9 μm for S3, respectively. On the other hand, length of the crystals in *c* direction was decreased from 32.9 to 18.4 μm with increasing KF molar ratios for S2 and S3, respectively.

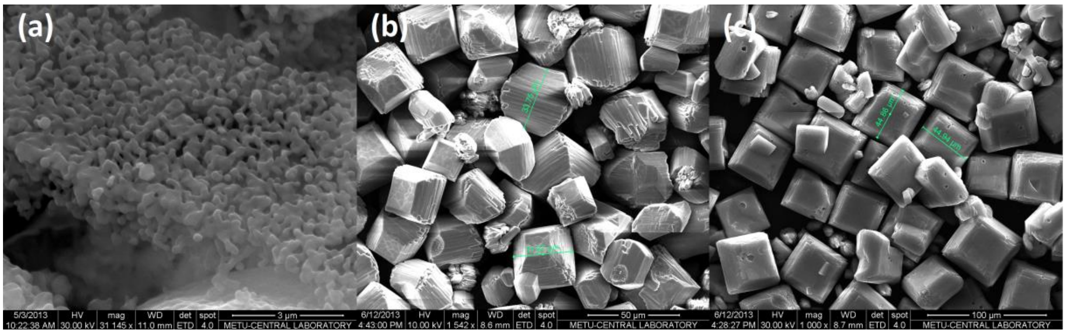

Figure 4.2. SEM images of S1 (a), S2 (b) and S3 (c). Molar ratios of KF are 0.09, 0.92 and 2.01, respectively.

The effect of changing amount of KF was investigated with a lower concentration of HCl; i.e. x=1.67, for samples S4-S6. Figure 4.3 shows XRD patterns of S4, S5 and S6. According to Figure 4.3, S5 and S6 synthesized with higher amount of KF; i.e. 0.92 and 2.01, respectively, possessed higher crystallinity compared to S4 synthesized with 0.09 M. However, quartz impurity formation was observed at higher fluoride ion concentration as observed in S2 and S3.

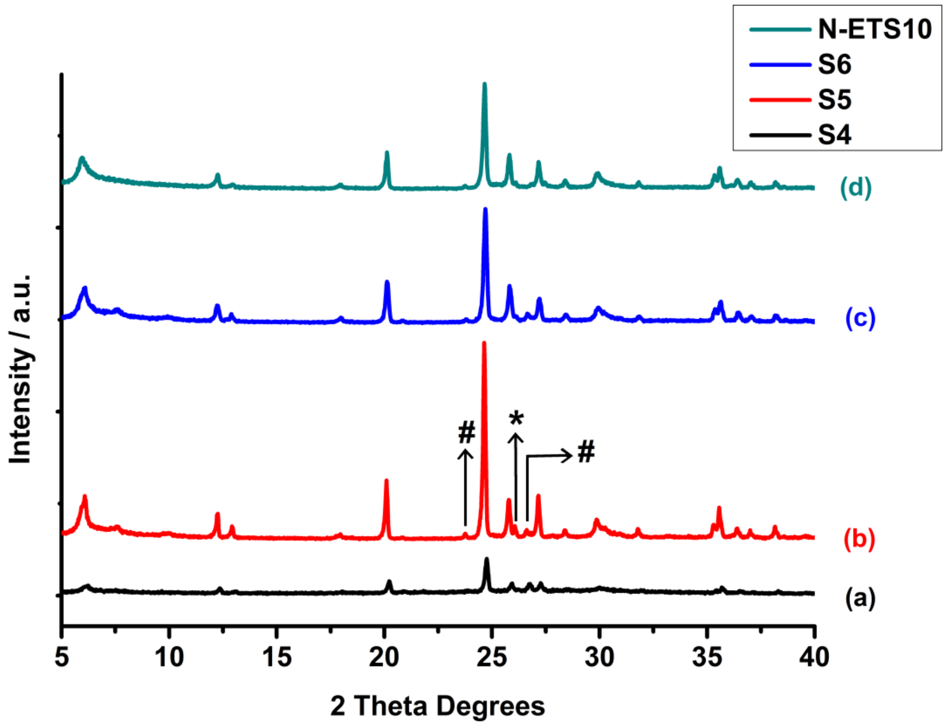

Figure 4.3. XRD patterns of M-ETS-10 (with 1.67 M HCl) with different KF molar ratio. The KF molar ratios are 0.09 for S4 (a), 0.92 for S5 (b) 2.0 for S6 (c) and N-ETS-10 (d). * indicates AM-3 formation and # indicates quartz formation.

Moreover, S1 and S4 contained the same amount of KF but different amount of HCl in reaction gels. Accordingly, although, S1 was amorphous, it can be seen that S4 was slightly crystalline. Lower amount of HCl might lead to an increase in the crystallinity of S4. Figure 4.3 shows that increase in amount of KF increased in the crystallinity for S5 and S6 as observed in XRD results of S2 and S3 (Figure 4.1). However, quartz and AM-3 impurity formation also increase with higher fluoride ion concentration.

SEM images of S5 and S6 showed that crystals have uniform size and almost dual elongated square bipyramid morphology (Figure 4.4). According to Table 4.1, upon the mole ratio of KF increased, length of *a* direction of the S5 and S6 crystals remained almost the same. Also, lengths of S5 crystals in *b* and *c* directions was 50 and 40 μm, respectively, whereas increase in KF amount caused a decrease in both *b* and *c* directions for S6 crystals; these were 44 and 18 μm, respectively.

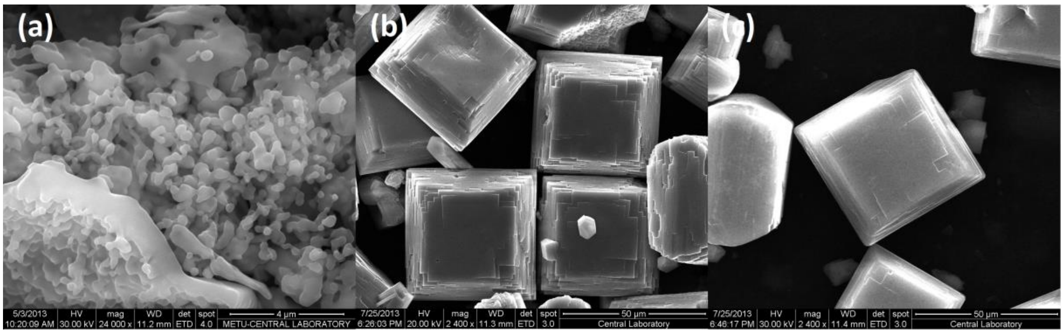

Figure 4.4. The SEM images of S4 (a), S5 (b) and S6 (c). The molar ratios of KF are 0.09, 0.92 and 2.01, respectively.

It is observed that changing KF content in synthesis gel directly controls both crystallinity and length of growth direction of ETS-10 crystals as also reported in the literature [10].

Furthermore, Table 4.1 also indicates that the amount of HCl in synthesis gel affected direction of the growth. Upon using 2.01 M KF, it seems that HCl amount did not effect on growth direction (S3 and S6). Although upon using 0.92

M KF, effect of HCl was obvious. The length of *a,b* and *c* directions of S5, synthesized with 1.67 M HCl, were larger than the length of all directions of S2, synthesized with 1.99 M HCl. It seems 1.67 M HCl content is more suitable for growth in all directions. The pH values of S5 and S2 were 10.3 and 10.6, respectively. Similar result was reported in previous study [75].

4.2 Synthesis of N-ETS-10

N-ETS-10 crystals, having 500-600 nm of size, were hydrothermally synthesized using gel composition of 3.4 Na_2O: 1.5 K_2O: TiO_2: 5.5 SiO_2: 150 H_2O [86]. The XRD pattern of N-ETS-10 as shown in Figure 4.5 consists of characteristic ETS-10 peaks. Consequently, all the obtained products matched the data reported for ETS-10 in the literature [8] indicating the purity of the crystals. .

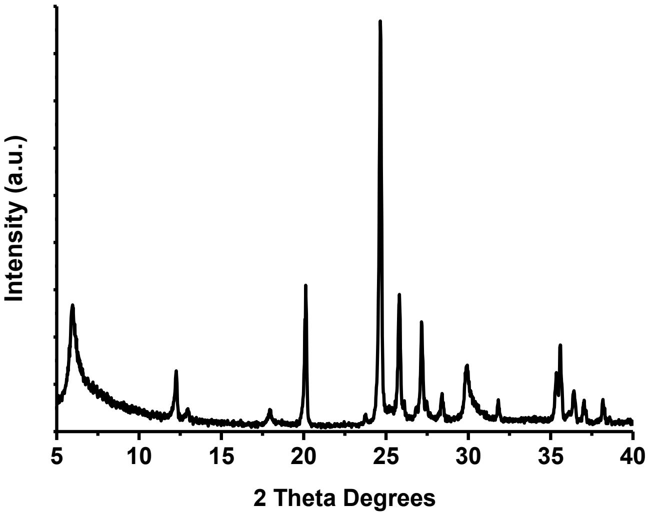

Figure 4.5. X-Ray Diffraction pattern of N-ETS-10.

Furthermore, Figure 4.6 shows FE-SEM images of N-ETS-10 crystals. The images revealed that the crystals had truncated bipyramid morphology with ~0.5 µm sized.

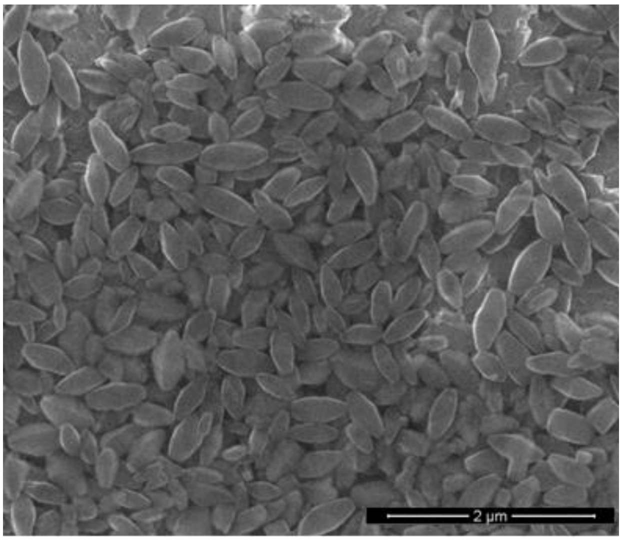

Figure 4.6. FE-SEM micrograph of N-ETS-10.

As a conclusion, several sized ETS-10 crystals; namely almost 36, 44, 50 μm and 500-600 nm, were successfully synthesized with different titanium source and acidic/alkaline components such as KF, H_2SO_4 and HCl. ETS-10 crystals with 500-600 nm size were used at post-treatment and ruthenium nanoparticle formation. Whereas ETS-10 crystals with 50 μm size were used in synthesis of $[Ru(bpy)_3]^{2+}$ and loading pyronine.

4.2.1 Modification of Crystal Structure of N-ETS-10 with Hydrogen peroxide and Sulfuric acid

The enlargement of micropores; i.e. forming supermicropores, in N-ETS-10 crystals was performed by post-synthesis treatment using two different concentration of aqueous H_2O_2 solution. Subsequently, each sample was exposed to aqueous H_2SO_4 solution for 4 hours to throw out the possible side products of H_2O_2 treatment and to prevent from stacking the channels of the crystals.

Figure 4.7 shows that the XRD patterns of N-ETS-10 samples before and after H_2O_2 (10wt.%(3) and 30wt.%(1)) and H_2SO_4 treatments. According to Figure 4.7, it can be seen that the XRD pattern of all samples match well with that of as-synthesized ETS-10 [8]. The relative crystallinities of treated samples were calculated using the sum of the intensities of the diffraction peaks at $2\Theta = 24.65$-$27.5°$ with respect to the original sample of which its crystallinity was assumed to be 100% (Table 4.2).

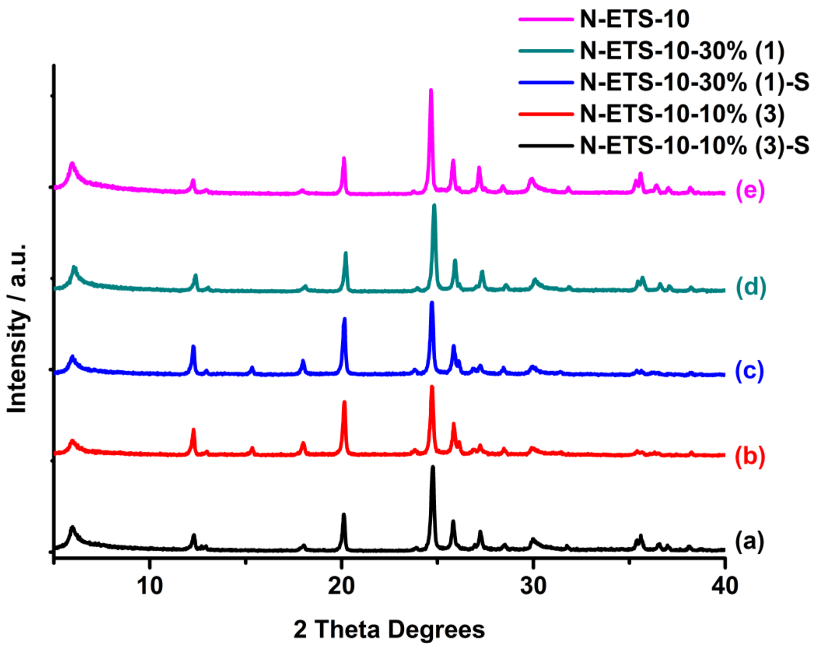

Figure 4.7. X-ray diffraction patterns of N-ETS-10 (e), the samples treated H_2O_2 (i.e., N-ETS-10-30%(1) (d) and N-ETS-10-10%(3) (b)) and the samples treated both H_2O_2 and H_2SO_4 (i.e., N-ETS-10-30%(1)-S (c) and N-ETS-10-10%(3)-A (a)).

As shown in Table 4.2, H_2O_2 treatment had less effect on crystallinity. However, both H_2O_2 and H_2SO_4 lead to a decrease in the crystallinity. Nevertheless the N-ETS-10 structure was conserved as also observed by SEM analyses (Appendix A).

Table 4.2. The variation in extra-framework cations, microporous area and volume after post-treatments.

System code	Na/Ti[a]	K/Ti[a]	S_{total} (m^2/g)[b]	S_{Ext} (m^2/g)[c]	$S_{MicroPore}$ (m^2/g)[c]	Pore Volume (cc/g)[d]	Pore Size (Å)[d]	Percent Cryst. (%)[e]
N-ETS-10	1.03	0.58	404.8	92.1	312.7	0.16	12.8	100
N-ETS-10-30%(1)	1.98	1.06	362.4	81.8	280.6	0.15	13.2	90.6
N-ETS-10-30%(1)-S	0	0	338.6	125.8	212.8	0.14	10.8	79.7
N-ETS-10-10%(3)	1.69	1.01	342.7	131.8	210.9	0.14	9.7	87.9
N-ETS-10-10%(3)-S	0.03	0	387.9	137.3	250.6	0.16	10.8	78.6

[a] Measured by ICP.
[b] Determined by Multipoint BET.
[c] Determined by t-plot Method.
[d] Determined by Saito-Foley (SF) Method.
[e] Calculated from [87].

Moreover, Table 4.2 shows the extra-framework cations to titanium ratios (Na/Ti and K/Ti ratios) for N-ETS-10 and all treated samples determined by ICP-MS analyses. The ratios at H_2O_2 treated samples is higher than N-ETS-10. This result indicates removal of Ti-O-Ti chains. Although, it is seen that Na/Ti and K/Ti ratios decreased after H_2SO_4 treatment of both H_2O_2 treated samples. It might be due to leaching not only Ti-O-Ti chains but also extra-framework cations. Yang and coworker indicated that acidic medium deforms zeolite matrix and so hydrogen cation; i.e. H^+, is replaced by other cations located in framewok [5]. In this study, it seems that H_2SO_4 has this effect of cation replacement on ETS-10. Indeed, it seems that H_2SO_4 treatment is more effective for leaching Na and K cations than Ti-O-Ti chains.

Table 4.2 indicates that all total surface area for all treated samples decreased. H_2SO_4 treatment applied to single step 30wt. % H_2O_2 treated ETS-10 (N-ETS-10-30%(1)-S) lead to further decrease in total surface area (338,6 m^2/g). However, same acid treatment applied to three step 10wt. % H_2O_2 treated ETS-10 (N-ETS-10-10%(3)) resulted in an increase of total surface area (387,9 m^2/g). Furthermore, it can be observed that the micropore surface area also increased for the same sample. Also, it was observed that single step 30wt. % H_2O_2 treatment (N-ETS-10-30%(1)) caused increase in pores size (13.2 Å). On the other hand, when acid was treated to same sample; that is N-ETS-10-30%(1)-S, pore size decreased to 10.8 Å. Moreover, it was observed that acid treatment caused to increase in pore size of N-ETS-10-10%(3)-S (9.7 Å) when compared to N-ETS-10-10%(3) (10.8 Å). Pavel *et al.* [54] applied the identical H_2O_2 treatment protocol to ETS-10, which is single step with 30 wt.% and three step with 10 wt.% H_2O_2 treatment. They concluded that 10 wt.% treatments results in more stable framework with less damage with respect to single step 30 wt.% treatment creating a more severely damaged ETS-10 structure. Accordingly, in the current study, the H_2SO_4 treatments might have caused further destruction of the more severely damaged framework (N-ETS-10-30%(1)) leading to further decrease in total surface area and micropore volume. On the other hand, the identical H_2SO_4 treatment seems to clean the less severely damaged ETS-10 framework (N-ETS-10-10%(3)) opening up this structure due to increase in pore size.

Similar conclusions can be made upon the nitrogen adsorption-desorption isotherms as seen in Figure 4.8. It can be seen from hysteresis loop at P/P_0= 0.6-0.95 (green line at Figure 4.8) that there is more significant mesopore form in N-ETS-10-30%(1) upon single harsh step H_2O_2 treatment suggesting again a more significant structural damage. Moreover, the volume adsorbed was observed to be maximum for N-ETS-10-10%(3)-S. Accordingly, the matrix seems to be the most suitable framework for nanoparticle formation. Ruthenium nanoparticle formation was investigated using N-ETS-10 and N-ETS-10-10%(3)-S.

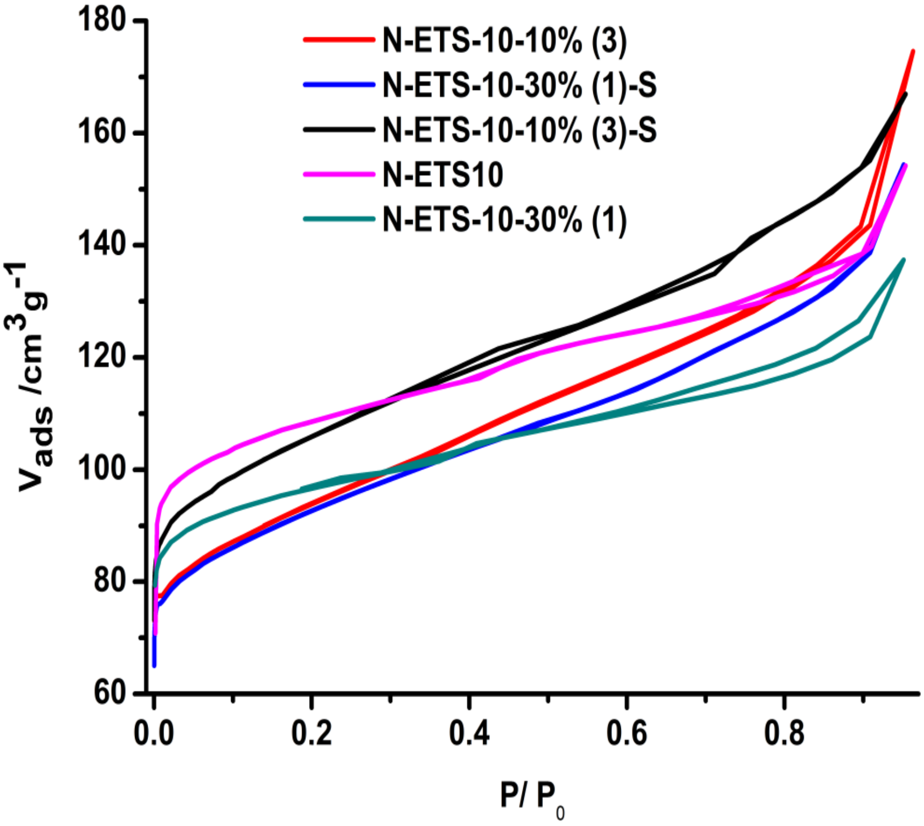

Figure 4.8. The nitrogen adsorption and desorption isotherms of N-ETS-10, the samples treated H_2O_2 (i.e., N-ETS-10-30%(1) and N-ETS-10-10%(3)) and the samples treated both H_2O_2 and H_2SO_4 (i.e., N-ETS-10-30%(1)-S and N-ETS-10-10%(3)-S).

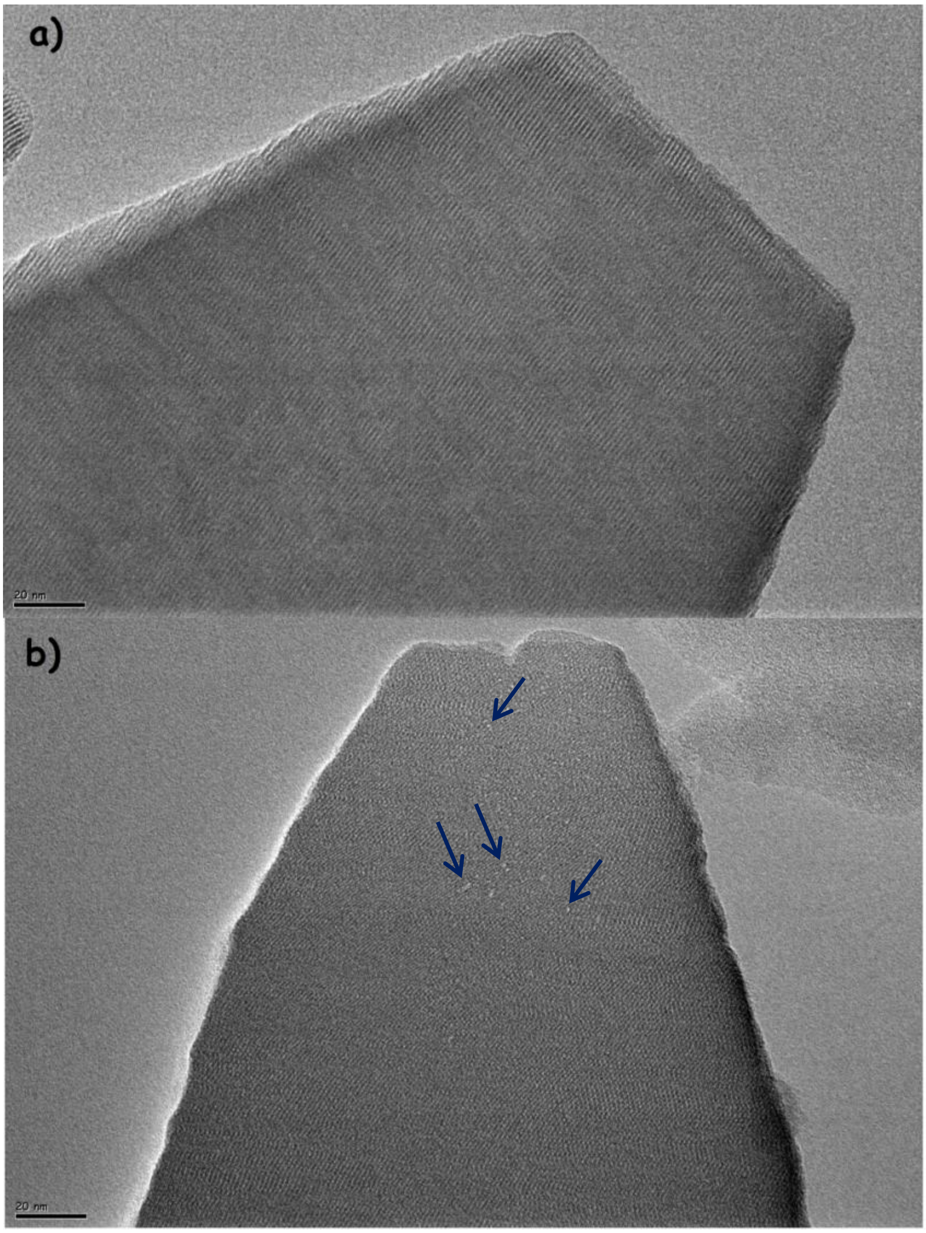

Figure 4.9. The HR-TEM images of N-ETS-10 (a) and N-ETS-10-10%(3) (b).

Figure 4.9 shows HR-TEM images of N-ETS-10 and N-ETS-10-10%(3)-S. There is no significant mesopores formation in N-ETS-10-10%(3)-S. The observed white spots can also be seen in N-ETS-10 due stacking faults formed through synthesis of ETS-10. Anderson *et. al* [6, 88] reported that ETS-10 crystals could be highly disordered and this circumstances resulted in stacking faults and defects in structure.

4.3. Synthesis and characterization of ruthenium(0) nanoparticles incorporated into ETS-10

Two consecutive steps were followed for preparation of ruthenium(0) nanoparticles. The first step is the ion-exchange procedure where ruthenium(III) chloride hydrate was used as the reagent and extra-framework cations; i.e. Na^+ and K^+, were exchanged with ruthenium cation; i.e. Ru^{3+}. The second step was the chemical reduction of Ru^{3+} cations with $NaBH_4$. Ruthenium(0) nanoparticles were aimed to be formed in N-ETS-10 and N-ETS-10-10%(3)-S samples. The aim was to investigate whether increased pore volume would result in any change in the formation of these nanoparticles in N-ETS-10-10%(3)-S.

Figure 4.10 shows the X-ray diffraction patterns of both ruthenium(0) incorporated into N-ETS-10 and post treated N-ETS-10-10%(3)-S. According to Figure 4.10, all peaks matched the as-synthesized ETS-10 peak positions and no additional peaks were observed. The results showed the intensity of 105 reflection increased in Ru-N-ETS-10-10%(3)-S; nevertheless, the intensities of other reflections decreased in this sample (Figure 4.10-a). From Table 4.2, ICP-MS results show that all extra-framework cations were removed after post-treatment. Consequently, ion-exchange could not be performed since extra-framework cations were absence instead impregnation of the ions were achieved at N-ETS-10-10%(3)-S. Thus, the sample was ruthenium nanoparticle impregnated N-ETS-10-10%(3)-S. The reason of increase in intensity of 105 reflection might be site selectivity during ruthenium(0) formation in ETS-10 since all specific plane orientations in ETS-10 structure are indicated with 2ϴ values.

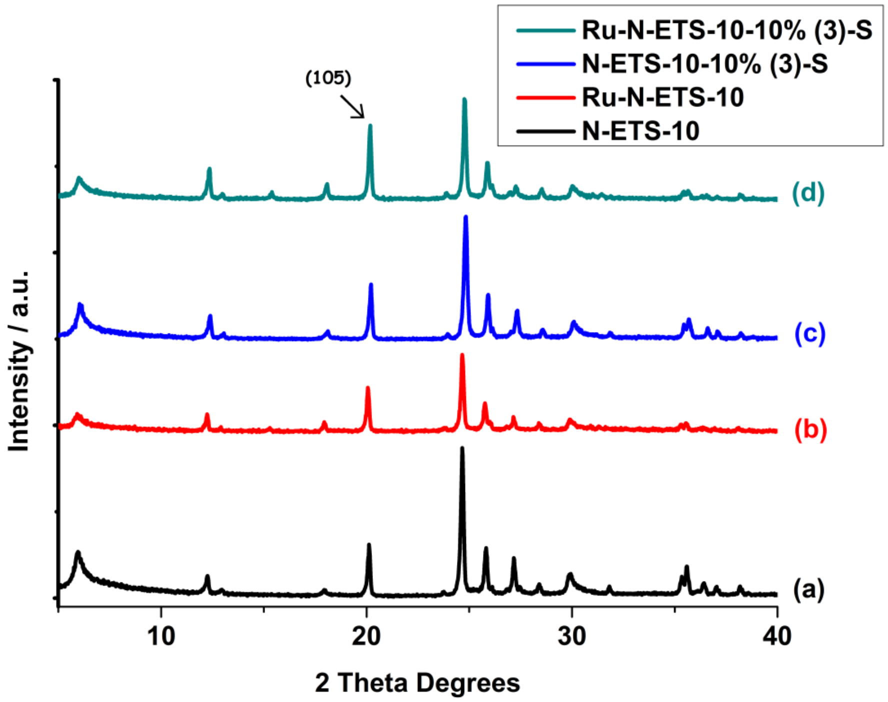

Figure 4.10. X-ray diffraction patterns of N-ETS-10 (a), ruthenium nanoparticle incorporated N-ETS-10 (b), treated N-ETS-10 (c) and ruthenium nanoparticle incorporated treated N-ETS-10(d), respectively.

Nitrogen adsorption-desorption isotherm results are shown in Table 4.3. The results revealed that the total, external, micropore surface areas, pore volume and pore size of N-ETS-10 decreased after the ruthenium nanoparticle formation. This decrease is most likely the result of localization of ruthenium nanoparticles in micropores of ETS-10 to some extent [8]. According to Table 4.3, it is observed that the noticeable increase in total surface area and micropore surface area in N-ETS-10-30% after ruthenium nanoparticle formation, whereas external surface area did not increase and pore size almost did not change. Figure 4.11 is HR-TEM images of N-ETS-10 and Ru-N-ETS-10. It is shown that ruthenium nanoparticles formation incorporated into ETS-10 matrix.

Table 4.3. Summary of textural properties of N-ETS-10, Ru nanoparticles incorporated ETS-10, modified ETS-10 and Ru nanoparticles of incorporated modified ETS-10.

System code	S_{total} (m^2/g)[a]	S_{Ext} (m^2/g)[b]	$S_{MicroPore}$ (m^2/g)[b]	Pore Volume (cc/g)[c]	Pore Size (Å)[c]
N-ETS-10	404.8	92.1	312.7	0.16	12.8
Ru-N-ETS-10	329.5	88.6	240.9	0.13	11.8
N-ETS-10-10%(3)-S	387.9	137.3	250.6	0.16	10.8
Ru-N-ETS-10-30%(1)-S	374.3	100.2	274.1	0.15	10.7

[a] Determined by Multipoint BET.
[b] Determined by t-plot Method.
[c] Determined by Saito-Foley (SF) Method.

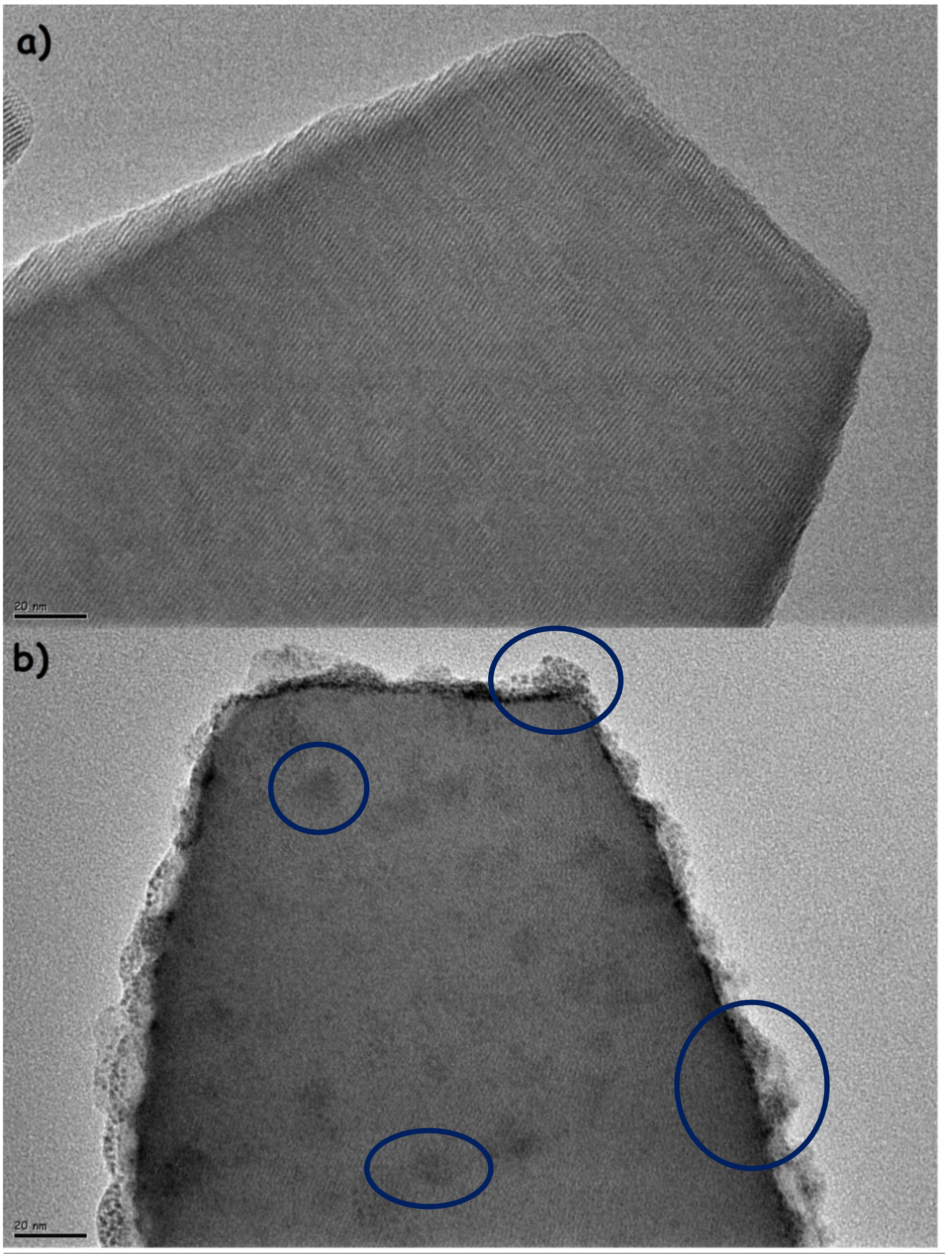

Figure 4.11. The HR-TEM images of N-ETS-10 (a) and Ru-N-ETS-10 (b).

It is known that post-treatment with certain chemicals, such as H_2O_2 and H_2SO_4, makes the framework more susceptible to defect formation by breaking bonds resulting into a less stable structure [56, 87]. Nanoparticle formation in such porous structures by themselves has a similar damaging role in the framework.

Sometimes these damages or defects are desired in certain applications. One way to recognize these damages in ETS-10 is Raman spectroscopy analysis where Ti-O-Ti shows a unique peak at 725 cm^{-1}. In the current study, this band was completely vanished (Appendix B) upon nanoparticle formation, although the peaks of characteristic XRD pattern still remained (Figure 4.10). Moreover, it seems that there was more significant nanoparticle formation in N-ETS-10-10%(3)-S, having the size with 2-5 nm, in the treated samples as opposed to N-ETS-10 from HR-TEM images (Figure 4.12).

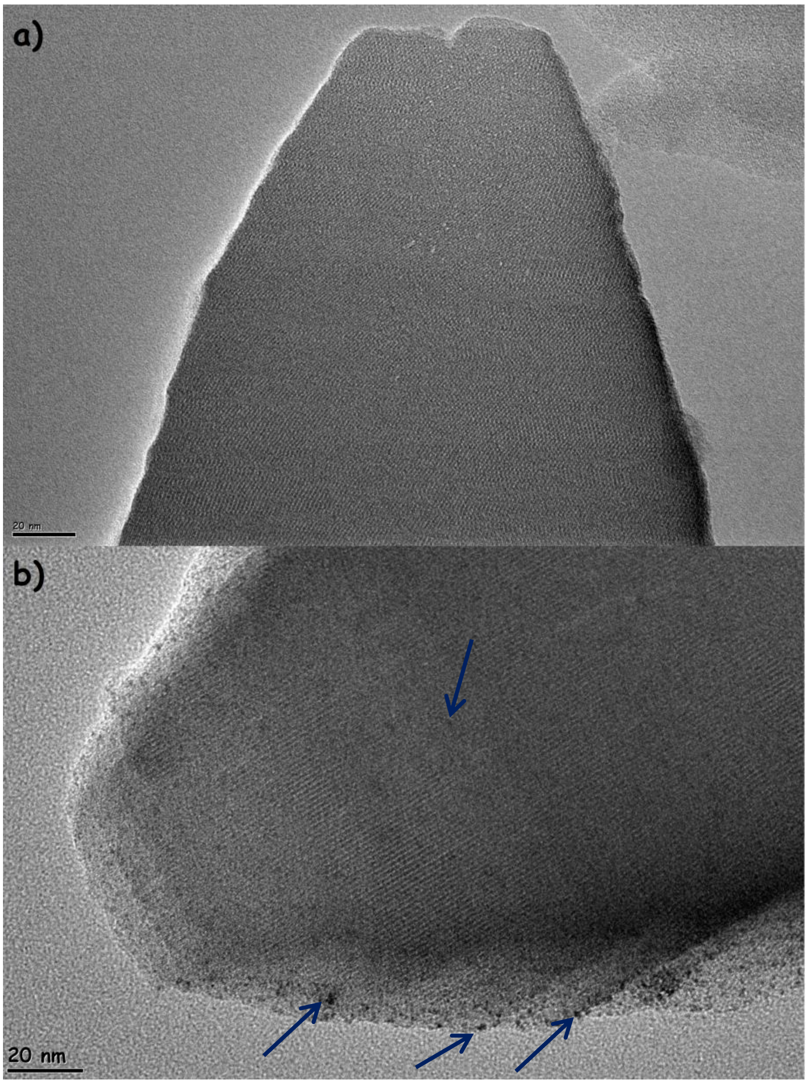

Figure.4.12. HR-TEM images of N-ETS-10-10%(3)-S (a) and Ru-N-ETS-10-10%(3)-S (b).

4.4 Dyes as guest / Zeolites as host for Host-Guest System

Cationic dye molecules and zeolite samples are used for host-guest assembly. Ship-in-a-bottle synthesis is prominent technique to form dye molecules, remarkable large sized as guest, inside of host material upon host material has not enough space let guest molecule effectively diffuse inside host material. Tris(2,2'-bipyridine)ruthenium(II) cation, spherical shape with diameter of 1.2 nm as seen in Figure 4.13, is one of the prevalent example of synthesized dyes inside zeolites through this method [31, 36].

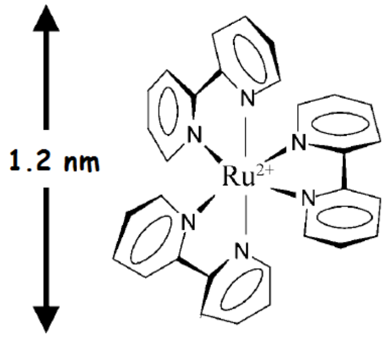

Figure 4.13. The chemical structure of $[Ru(bpy)_3]^{2+}$. Adapted from [39].

Although, the size of the dye molecule is larger than sodalite cages of zeolite Y , it can be successfully formed in supercages of zeolite-Y as shown in the literature [64], which has a supercage in its framework (Figure 1.3). Accordingly, in the current study, both M-ETS-10 and zeolite Y were investigated as host materials for forming tris(2,2'-bipyridine)ruthenium(II) cation, an organometallic dye molecules. M-ETS-10 with 50x44x18 µm size; i.e. S6, was preferred over N-ETS-10 with 500 nm size, in order to obtain more recognizable images from optical microscopy studies. Tris(2,2'-bipyridine)ruthenium(II) cation is denoted as

Ru(bpy) in this section. Moreover, pyronine, a linear organic dye molecule, which was assumed to easily penetrate into the frameworks was loaded into M-ETS-10.

4.4.1 Synthesis and Characterization of tris(2,2'-bipyridyl)ruthenium(II) incorporated into ETS-10

Synthesis of tris(2'2-bipyridyl)ruthenium(II) cations (Ru(bpy)) contains two consecutive procedures and was applied by using two different ruthenium sources. The first source for ion-exchange is hexaamineruthenium(III) chloride; i.e. $[Ru(NH)_6]Cl_{3,}$ which was added into the aqueous M-ETS-10 solution and stirred at room temperature (denoted as RuNH-M-ETS-10). The second source is ruthenium(III) chloride hydrate; i.e. $RuCl_3.nH_2O$, which was used instead of hexamine ruthenium(III) chloride for another trial (denoted as Ru-M-ETS-10). Typical ion-exchange procedure was applied. After this procedure, extra framework cations of ETS-10; i.e. Na^+, were exchanged with $[Ru(NH)_3]^{3+}$ and Ru^{3+} cations resulting in RuNH-M-ETS-10 and Ru-M-ETS-10 samples, respectively. For the second step of the procedure, $[Ru(NH)_3]^{3+}$ and Ru^{3+} cations were let to react in the ETS-10 framework with 2'2-bipyridyl in ethanol solution using a reflux system at room temperature for 4 hours followed by immediate stirring at 200 °C for 24 hours.

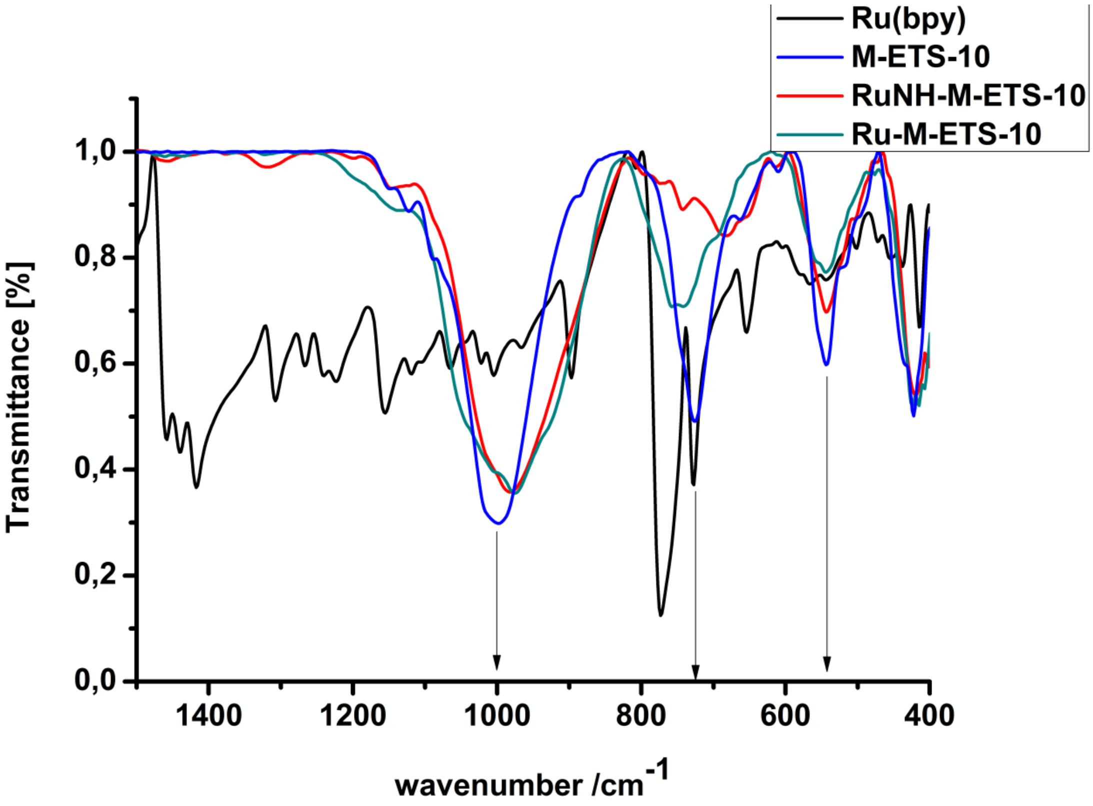

Figure 4.14. FTIR spectra of Ru(bpy) (black line), M-ETS-10 (blue line), RuNH-M-ETS-10 (red line) and Ru-M-ETS-10 (green line) in the frequency range of 400-1500 cm^{-1}.

Figure 4.14 shows the FTIR spectra of commercial Ru(bpy), M-ETS-10, RuNH-M-ETS-10 and Ru-M-ETS-10 in the frequency range of 400-1500 cm^{-1}. The band at 725 cm^{-1} is assigned to the Ti-O stretching mode of ETS-10. It seems that the most noticeable difference upon Ru(bpy) formation leads to a change in the frequency and the intensity of this particular band. In another study, the decrease in the intensity of this peak was assigned to the Ti vacancies in the Ti-O-Ti chains [8]. Accordingly, it seems that this formation of Ru(bpy) affected the Ti-O-Ti chains. It was observed that intensity of sharp band at 545 cm^{-1}, indicating Si-O rocking and O-Ti-O bending vibrations in ETS-10 crystals, decreased. It could be due to affected Ti-O-Ti chains.

A sharp band at 1000 cm^{-1} indicating Si-O stretching vibrations in ETS-10 crystals was observed, which was broadened for samples RuNH-M-ETS-10 and Ru-M-ETS-10. The bands between 900 and 1500 cm^{-1} show aromatic C-N and C=C stretching bands [89]. Therefore, this can be due to overlapping of this sharp band with aromatic C-H vibrations in $[Ru(bpy)_3]^{2+}$ molecules.

UV-Vis spectroscopy is extensively used for dye analysis due to their properties of obvious and characteristic absorbance in UV and visible range of electromagnetic spectrum.

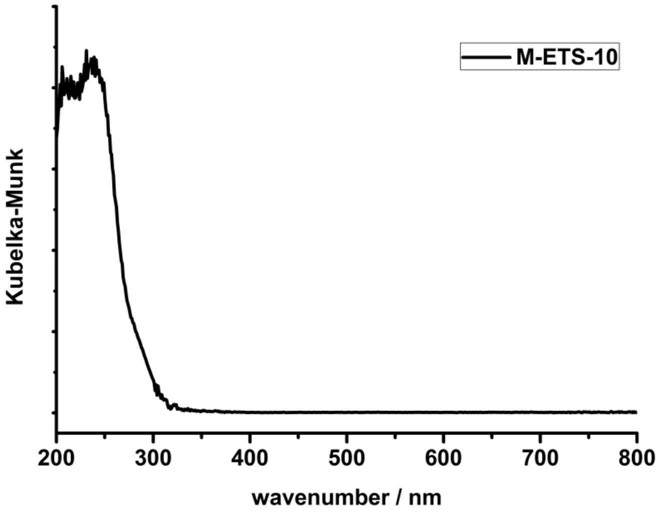

Figure 4.15. UV-Vis spectrum of M-ETS-10.

Figure 4.15 shows the UV-Vis absorption spectrum of M-ETS-10. A broad absorption band in a frequency range of 200-350 nm can be seen due to two main absorption bands. These bands are caused by by ligand-to-metal-charge-transfer (LMCT) transitions of two types of oxygen ligands; namely, Ti-O-Ti at 282 nm and Si-O-Ti at 214 nm [13]. Moreover, there is no absorption band at the visible region of the spectrum.

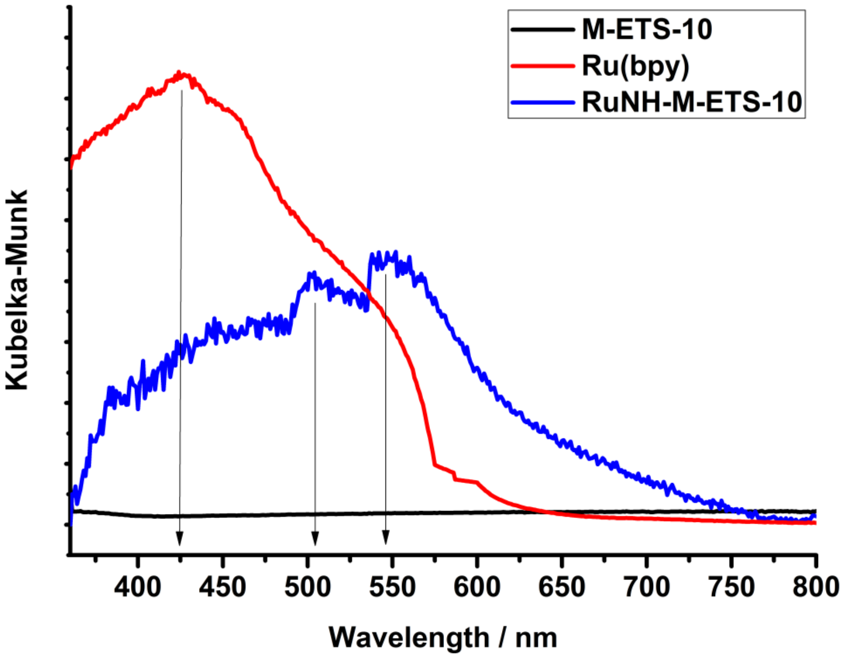

Figure 4.16. UV-Vis spectra of Ru(bpy) (black line), M-ETS-10 (green line), RuNH-M-ETS-10 (red line) and RuNH-M-ETS-10 (blue line).

Figure 4.16 shows UV-Vis spectra of Ru(bpy), M-ETS-10 and RuNH-M-ETS-10. Ru(bpy) has a characteristic absorption maximum at 427 nm due to metal-to-ligand ($t_2 \rightarrow \pi^*$) charge transition [60]. It was reported that the characteristic absorbance at 427 could be shifted to longer wavelength for samples consisting of $[Ru(bpy)_3]^{2+}$ and zeolite due to cage structures of zeolites [31,32]. Moreover, according to Dewilde and coworkers [60], low $[Ru(bpy)_3]^{2+}$ concentration in zeolite matrix causes another charge transition of Ru(bpy) at 550 nm; i.e. singlet-to-triplet transition, due to spin-orbit coupling. This transition is generally forbidden by spin-selection rule [60]. According to Figure 4.16, UV-Vis spectrum of RuNH-M-ETS-10 indicates $t_2 \rightarrow \pi^*$ transition of $[Ru(bpy)_3]^{2+}$ at 505 nm with an additional maximum at 550 nm. These results suggest that $[Ru(bpy)_3]^{2+}$ was formed in M-ETS-10 matrix but the efficiency of synthesis was low. Therefore, an absorbance maximum of singlet-to-triplet was also observed. It should also be added that. An obvious absorbance maximum from the obtained UV-Vis spectrum could not be obtained for Ru-M-ETS-10 as shown in Appendix C. These results suggest that the source used for forming the ruthenium dye molecule makes a significant difference once the zeolites are aimed to use as host materials.

Dyes have strong emission upon they are excited at proper wavelength. Therefore, light and fluorescence microcopies were performed to detect whether $[Ru(bpy)_3]^{2+}$ were synthesized incorporated into ETS-10 with different ruthenium sources or not. Figure 4.17-a shows the true color light microscopy image of RuNH-M-ETS-10 and a 30 μm sized ETS -10 crystal can be seen in this figure. Figure 4.17-b indicates true color fluorescence microscopy image of the same ETS-10 crystal. The sample was excited at 477 nm and emission of the excited sample was collected in the range between 500-800 nm. Although zeolites and zeo-type material are not fluorescent substances, there was a slight emission in the upper edge of RuNH-M-ETS-10 crystal. However, no emission could be obtained upon Ru-M-ETS-10 was excited at 477 nm.

According to the previous analysis, it was expected that the probability of $[Ru(bpy)_3]^{2+}$ formation was more successful by using $[Ru(NH)_6]^{3+}$ source than the Ru^{3+} source. This can be due to the fact that the structure of $[Ru(NH)_6]^{3+}$ is more similar to $[Ru(bpy)_3]^{2+}$. Ruthenium cations are already part of a coordination complex, which are covered with ammonia ligands through octahedral sites.

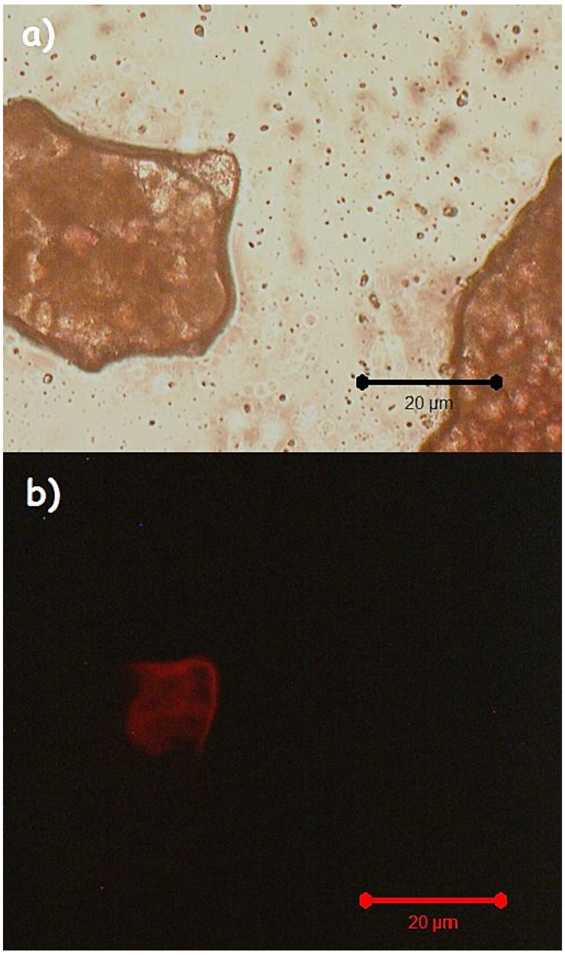

Figure 4.17. Light microscopy (a) and fluorescence microscopy (b) images of RuNH-M-ETS-10.

4.4.2 Synthesis and Characterization of tris(2,2'-bipyridyl)ruthenium(II) incorporated into ZeoliteY

$[Ru(bpy)_3]^{2+}$ was also synthesized in zeolite Y matrix as also illustrated in previous studies [31, 36]. Zeolite Y used for this reaction was already synthesized in our group [78]. The product synthesized with $[Ru(NH)_6]Cl_2$ as ruthenium source was denoted as RuNH-ZeoY.

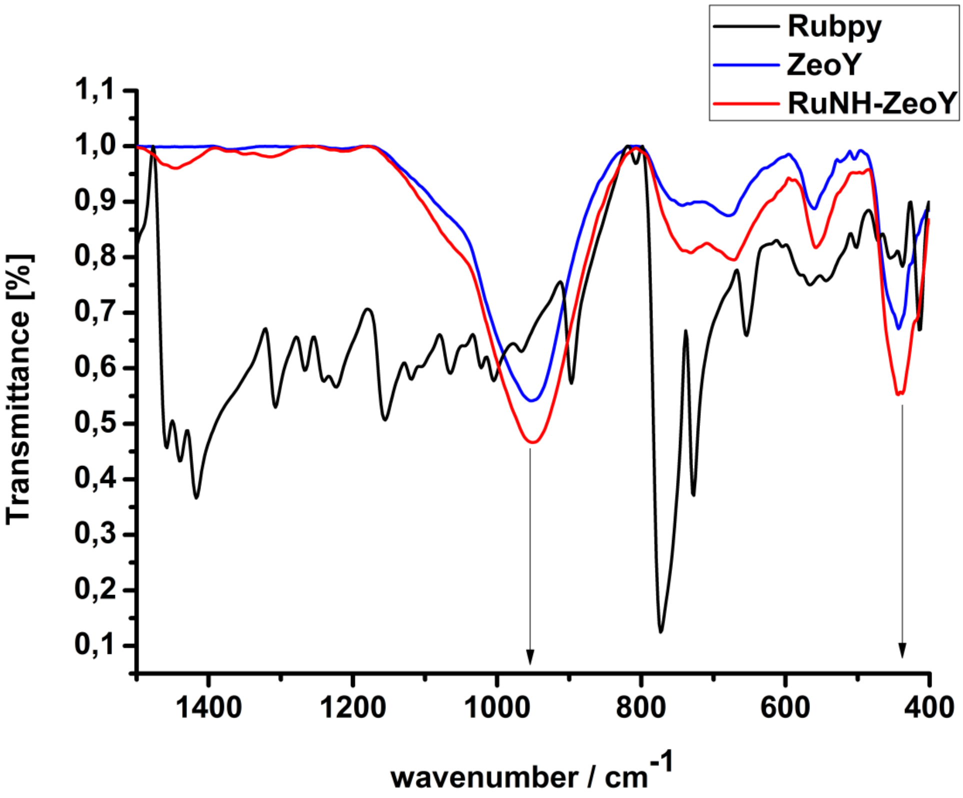

Figure 4.18. FTIR spectra of Ru(bpy) (black line), zeolite Y (blue line) and RuNH-ZeoY (red line) at between 400 and 1500 cm^{-1}.

Figure 4.18 shows the FTIR spectra of commercial Ru(bpy), zeolite Y, and RuNH-ZeoY in the frequency range of 400-1500 cm^{-1}. The band at 430 cm^{-1} is assigned to the bending vibrations of Si-O and Al-O in zeolite Y. A sharp band at 965 cm^{-1} indicates Si-O stretching vibrations in zeolite Y crystals. According to Figure 4.18, the entire characteristic bands in zeolite Y exist in the tested samples. In general, it seems that the main peaks still remain with a slight increase in intensity in the Ru-NH-ZeoY sample. Furthermore, there are new peaks with small intensity in the region of 1100-1400 cm^{-1} region. Thus the dye incorporation, although in slight amount, seems to have caused new interactions in the zeolite Y framework.

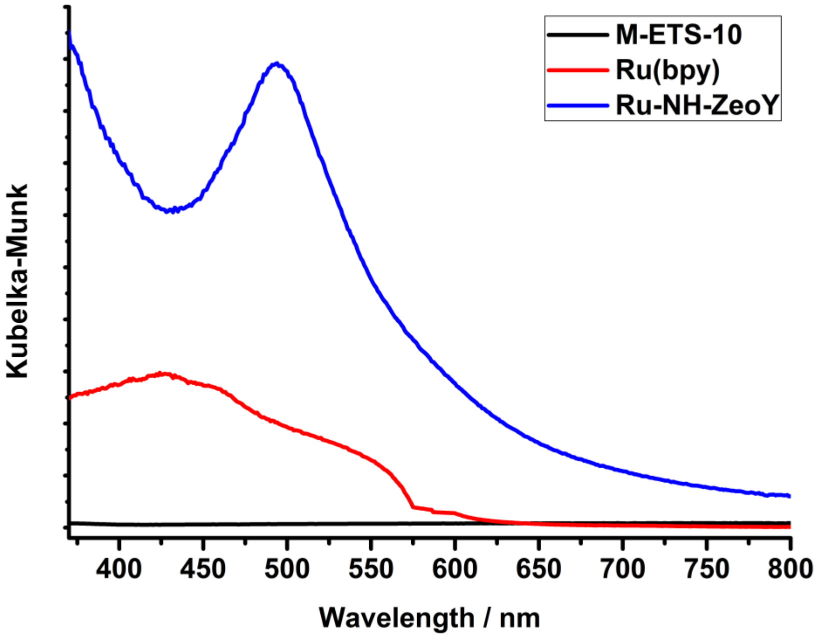

Figure 4.19. UV-Vis spectra of zeolite Y (black line), Ru(bpy) (red line) and RuNH-ZeoY (blue line).

Figure 4.19 indicates UV-Vis spectra of commercial Ru(bpy), zeolite Y and RuNH-ZeoY. According to Figure 4.19, the peak at 500 nm can be significantly observed upon $[Ru(bpy)_3]^{2+}$ formation in the matrix, whereas there is no absorbance in the spectrum of as-synthesized zeolite Y. Bossmann *et al.* [31, 32] observed that there was a redshift in $t_2 \rightarrow \pi^*$ transition in UV-Vis spectrum of the product upon compared to the one of aqueous commercial Ru(bpy). This result was associated with the shift in redox potential of Ru^{3+}/ Ru^{2+} couple within zeolite.

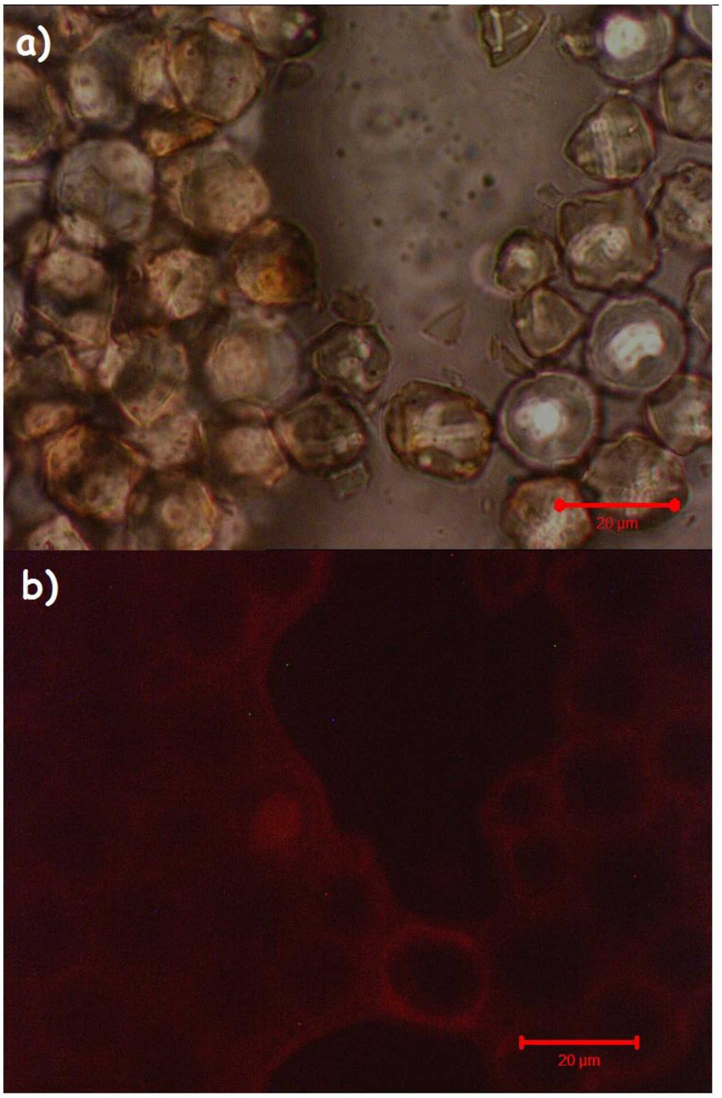

Figure 4.20. Light microscopy (a) and fluorescence microscopy (b) images of RuNH-ZeoY

True color light and fluorescence microcopy images are shown in Figure 4.20-a and Figure 4.20-b, respectively. Both images were formed from the same collected data, and thus the crystals observed at Figure 4.20-a and Figure 4.20-b belong to identical crystals. From Figure 4.17, one can conclude that the synthesis of the $[Ru(bpy)_3]^{2+}$ incorporated with zeolite Y according to the followed procedure was successful. The only region that these dye molecules can form should be the interior of the matrix, since the ion-exchange process occurs there, however the synthesized dye molecules give emission at the exterior surface of the crystals. Thus, it is reasonable to assume that $[Ru(bpy)_3]^{2+}$ were formed inside crystals but near the surface of the crystals or Ru^{3+} ions diffused out during the application and the dye molecules directly formed in the exterior surface of the crystals.

Furthermore, confocal laser scanning microscopy (CLSM) was performed in order to better obtain an image of the product. Figure 4.21 shows an image obtained by CLSM of RuNH-ZeoY. The obvious emission at the exterior surface can be seen giving the features of zeolite Y crystals, which again suggests the dye formation at the exterior surface.

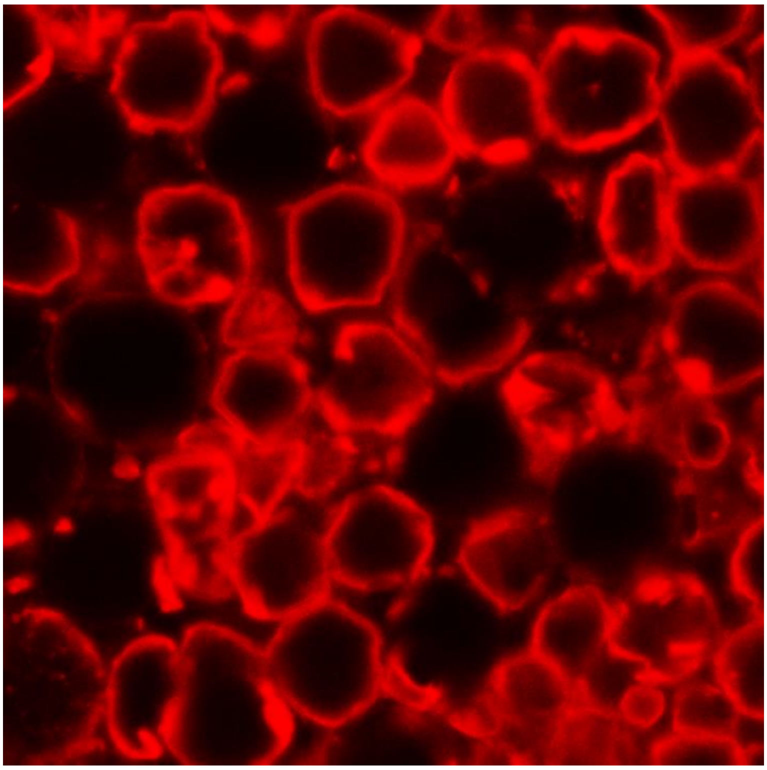

Figure 4.21. CLSM image of RuNH-ZeoY.

4.4.3 Loading cationic dyes to M-ETS-10

Another method of dye incorporated into zeolite is loading commercial dye molecules into the zeolite matrix, rather than ship-in-a-bottle method. In this method, small sized dye molecules, such as pyronine could easily be inserted by reflux method. Figure 4.22 shows the chemical structure of pyronine molecule, which is an aromatic linear cation. Linearity of pyronine lets it become more suitable for it to diffuse through the host materials

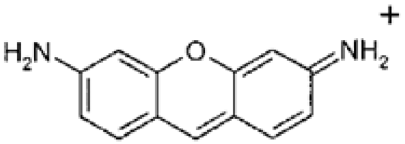

Figure 4.22. The chemical structure of pyronine molecule.

Figure 4.23 shows true color fluorescence microscopy image of pyronine loaded M-ETS-10. The image is from the top of an M-ETS-10 crystal. An apparent emission of the crystal can be observed from Figure 4.23 indicating the inclusion of pyronine into ETS-10.

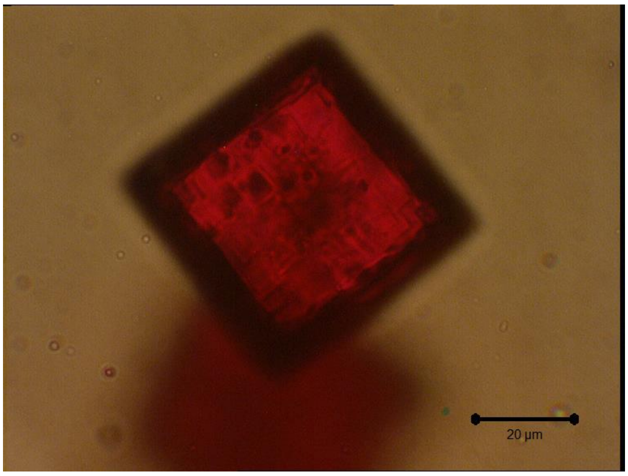

Figure 4.23. Fluorescence microscopy image of pyronine loaded M-ETS-10.

Figure 4.24 shows CLSM images pyronine loaded M-ETS-10 with the sample code of S3 having particle size of *a*=44.8, *b*=44.9, *c*=18.4 μm. The data was collected at every 2 μm through *z* direction corresponding *c* axis of the M-ETS-10 crystal. Data was collected from 26 μm to 2 μm. In these sequence images shown in Figure 4.24, it can be observed that pyronine penetrated into the M-ETS-10 channels. In Figure 4.24, every data collected was labeled at the bottom-right corner, indicating where detector collected data in *z* direction. At *z: 26 μm*, detector was out of focus. At *z: 16 μm*, detector scanned the top of the crystal. At *z: 12 μm,* detector scanned middle part of 3D crystal. It is indicative that there is no any emission at the center of image. At *z: 8 μm,* detector collected data only from near edges of the crystals. And at *z: 2 μm,* it is the last slide which detector could collect data. In Figure 4.24, it is seen that, at the center part of the crystal; i. e. at *z: 12 μm,* penetration of pyronine through M-ETS-10 crystal from *a* and *b* axis was almost uniform and pyronine molecules could not reach to the center of the crystal, at which there is no emission. Calzaferri and coworkers [26-27] reported that pyronine molecules were inserted to all channels of zeolite L crystals, having size almost 1 μm- 5 μm, at reflux for 4 hours. Reflux time could be sufficient for almost 45 μm sized M-ETS-10 in this experiment. Furthermore, several studies will be performed experiments in order to determine factors affected penetration length in the next years.

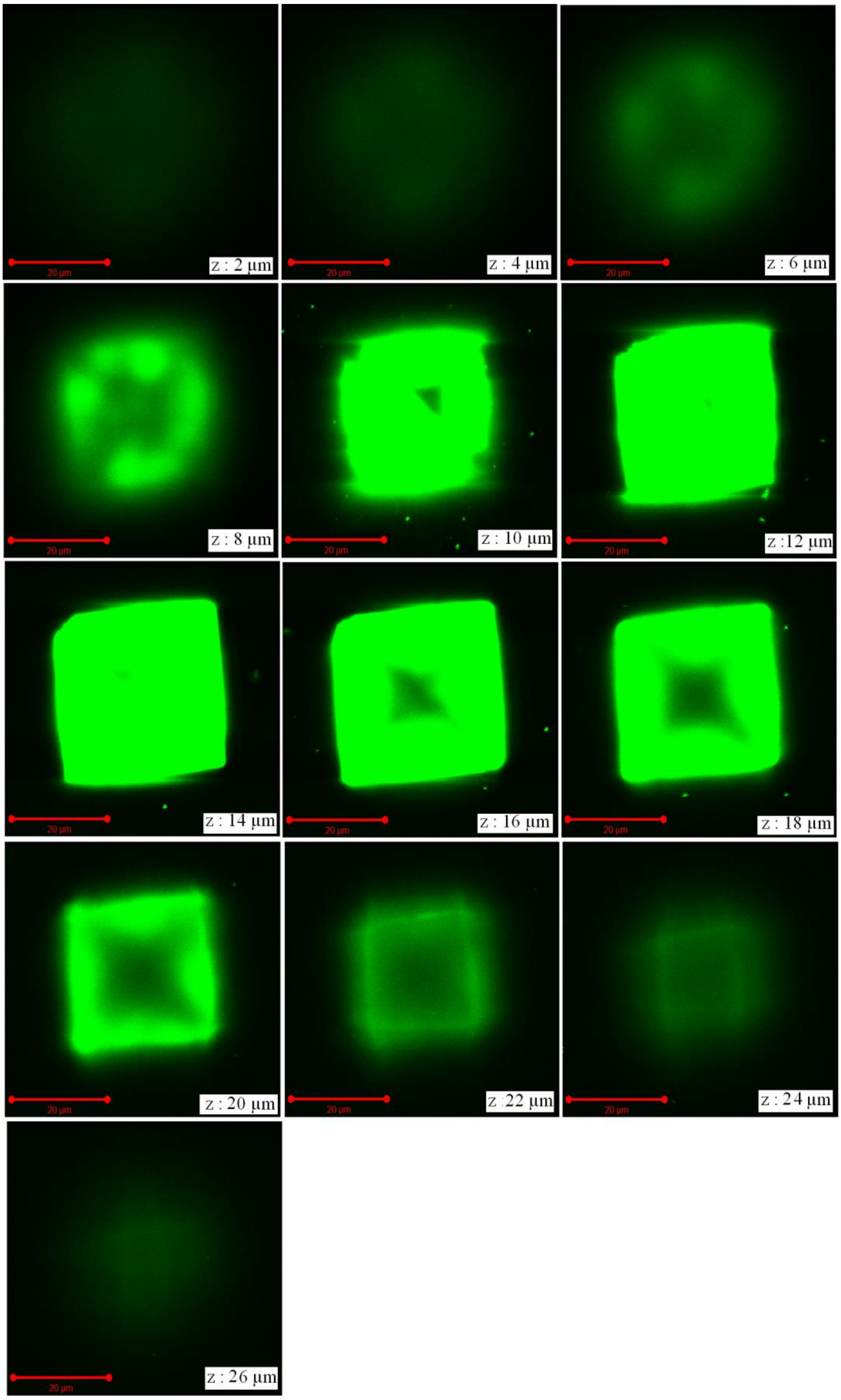

Figure 4.24. CLSM image of pyronine loaded M-ETS-10.

In summary, $[Ru(bpy)_3]^{2+}$ cationic dye molecules were synthesized following a typical ship-in- bottle synthesis route incorporated with ETS-10 for the first time. These studies were also conducted using zeolite Y, which can easily be found in the literature. FTIR studies indicated that there had been changes in the typical characteristic vibrations upon forming the dye molecule in the zeolite matrix. UV

-Vis results showed more significantly that these dye molecules were indeed formed upon following the synthesis route. Furthermore, it was seen that the source used for the dye molecule infect effects the product. Accordingly, it was seen that emission of RuNH-M-ETS-10 was less than RuNH-ZeoY, and Ru-M-ETS-10 had no emission. The difference of this efficiency might be caused by the difference in framework of M-ETS-10 and zeolite Y.

Moreover, it was observed that the samples loaded by commercial pyronine dye molecules with respect to the synthesized $[Ru(bpy)_3]^{2+}$ by ship-in-a-bottle synthesis had more emission. It was an expected result, since pyronine is much smaller than $[Ru(bpy)_3]^{2+}$, which even for the highest loading only an amount of 50% yield was obtained from previous studies using zeolite Y [66]. It is also possible that 2,2'-bipyridylmolecules have easier access to the exterior portion of the crystals and that they might have formed $[Ru(bpy)_3]^{2+}$ molecules at these regions. This formation might prevent the contact of 2,2'-bipyridyl molecules with ruthenium cations, which is the only route to form the dye molecules, leading to a significant decrease in the yield of formation and only a slight emission around the exterior surface of the crystals.

CHAPTER 5

CONCLUSIONS

In this study, ETS-10 crystals having a unique feature of possessing two dimensional Ti-O-Ti quantum wires in its structure were synthesized with two different morphologies and then tested as a host-material for ruthenium nanoparticles or organometallic dye molecules.

Post- treated ETS-10 with 500 nm particle size was used as a host material for host-guest system to investigate the effect of defect formation of inside the crystals for ruthenium nanoparticle formation. Post-treatment of ETS-10 crystals was applied by consecutive H_2O_2 and H_2SO_4 exposure, which seems to have resulted in a less stable structure of ETS-10. H_2SO_4 treatment might have caused further destruction of the more severely damaged framework for the sample treated 30 wt.% H_2O_2 solution once. On the other hand, the identical H_2SO_4 treatment seems to clean the less severely damaged ETS-10 framework for the sample treated 10 wt.% H_2O_2 solution three times, which opens up this structure.

Besides that, ruthenium nanoparticle formation, which is known to also damage the ETS-10 structure, caused further instability in the post-treated ETS-10 samples (N-ETS-10-10%(3)-S). Moreover, it seems that there was more significant nanoparticle formation with a particle-size distribution of 2-5 nm in the post-treated sample as opposed to the as-synthesized sample (N-ETS-10) as observed from the HR-TEM images.

Furthermore, ETS-10 crystals with several particle sizes of a x b x c μm were synthesized altering HCl and KF concentrations in molar formula of ETS-10. For the samples consisting of higher HCl (1.99 M) in the reaction gel; i.e. S2 and S3, effect of the KF amount in growth direction is more obvious, which resulted in an increase in a and b but decrease in c directions with increasing KF amount. However, for the samples consisting of lower HCl (1.67 M) in the reaction gel; i.e. S5 and S6, it was shown that KF amount has only a slight effect in the direction of growth. Increase in KF amount resulted in almost no change in a, a slight decrease in b and a sharp decrease in c directions.

Furthermore, dye molecules incorporated into ETS-10 crystals were performed as host-guest systems using two different procedures. Tris(2,2'-bipyridiyl)ruthenium(II) cation; i.e. $[Ru(bpy)_3]^{2+}$, was synthesized in the ETS-10 matrix using two different ruthenium sources; namely, $[Ru(NH)_6]Cl_2$ and $RuCl_2$ through ship-in-a-bottle synthesis.

It seems that the most noticeable difference upon $[Ru(bpy)_3]^{2+}$ formation leads to a change in the frequency and the intensity of this particular Ti-O stretching mode of ETS-10 in FT-IR spectrum. From UV-Vis spectra, a broad absorption band at about 500 nm, which is indicative of $t_2 \rightarrow \pi^*$ transition of $[Ru(bpy)_3]^{2+}$, in the sample synthesized with $[Ru(NH)_6]Cl_2$; i.e. RuNH-M-ETS-10, was observed. No absorption was detected in the sample synthesized using the $RuCl_3$ source; i.e. Ru-M-ETS-10. These results, in combination with the FTIR and UV-Vis studies suggest that the choice of $[Ru(NH)_6]^{3+}$ source rather than Ru^{3+} source lead to a more successful formation of the dye molecule incorporated with the zeolite matrix. This might be due to similar structure of $[Ru(NH)_6]^{3+}$ which results in an efficient formation of $[Ru(bpy)_3]^{2+}$. Although slight emission was detected by optical fluorescence microscopy, and no emission was detected by confocal laser scanning microscopy (CLSM), UV-Vis spectroscopy results proved the formation of dye molecules within the ETS-10 crystals, The slight fluorescent can be due to the low yield of the synthesis procedure; however all results obtained upon using

RuNH-M-ETS-10 suggests that the synthesis of this dye was achieved successfully using ETS-10 for the first time. Improvement of reaction yield will be examined in future studies.

Ship-in-a-bottle synthesis of $[Ru(bpy)_3]^{2+}$ was also applied into zeolite Y. It was observed apparent sharp absorbance maxima at 500 nm, which is indicative that the synthesis was completed successfully. Also, light fluorescence and CLSM images of the synthesized dye incorporated into zeolite Y indicates presence of dye molecules incorporated into zeolite Y noticeably.

Moreover, pyronine, a linear organic dye molecule, which was assumed to easily penetrate into the framework, was loaded into M-ETS-10. Penetration of pyronine was observed by CLSM. High emission was detected by CLSM from the regions of pyronine penetrating into M-ETS-10 crystal. It was observed that pyronine molecules could not reach at the center of ETS-10 crystal. The length of pyronine penetration can be adjustable by controlling the loading conditions such as reflux temperature and time.

The purpose of future studies will be to enhance performance of ship-in-a-bottle synthesis and control penetration of cationic dye molecules such as pyronine in ETS-10 matrix for various applications.

REFERENCES

[1] P. Payra, P.K. Dutta, in: S.M. Auerbach, K.A. Carrado, P.K. Dutta (Eds.), Handbook of Zeolite Science and Technology, Marcel Dekker, Inc., New York, 2003, p. 1.

[2] R. Xu, W. Pang, J. Yu, Q. Huo, J. Chen, *Chemistry of Zeolites and Related Porous Materials: Synthesis and Structure*, Wiley, 23, 2007.

[3] J. Rocha, M. W. Anderson, *Microporous Titanosilicates and Other Novel Mixed Octahedral-Tetrahedral Framework Oxides*, European Journal of Inorganic Chemistry, 801-818, 2000.

[4] Kuznicki, S.M. US Patent No. 4853202, 1989.

[5] C. Yang, Q. Xu, *States Of Aluminum in Zeolite β and Influence of Acidic or Basic Medium,* Zeolites, 19, 404-410, 1997

[6] M. W. Anderson, O. Terasaki, T. Ohsuna, A. Philippou, S. P. MacKay, A. Ferreira, J. Rocha, S. Lidi, *Structure Of The Microporous Titanosilicate ETS-10*, Nature, 367, 347-351, 1994.

[7] P. D. Southon, R. F. Howe, *Spectroscopic Studies of Disorder in the Microporous Titanosilicate ETS-10*, Chemistry of Materials, 14, 4209-4218, 2002.

[8] S. Galioğlu, M. Zahmakıran, Y. E. Kalay, S. Özkar, B. Akata, *Effect of silver encapsulation on the local structure of titanosilicate ETS-10*, Microporous and Mesoporous Materials, 159, 1–8, 2012.

[9] A. M. Zimmerman, D. J. Doren, *Electronic and Geometric Properties of ETS10 QMMM Studies of Cluster Models*, Journal of Physical Chemistry B, 110, 8959-8964, 2006.

[10] Z. Ji, M.N. Ismail, D.M. Callahan Jr., E. Pandowo, Z. Cai, T.L. Goodrich, K.S. Ziemer, J. Warzywoda, A. Sacco Jr., *The role of silver nanoparticles on silver modified titanosilicate ETS-10 in visible light photocatalysis*, Applied Catalysis B: Environmental, 102, 323–333, 2011.

[11] Sezin Galioglu, Melda Isler, Zeynep Demircioğlu, Mehmet Koç, Francis Vocanson, Nathalie Destouches, Raşit Turan, Burcu Akata, *Photochromic Behavior of Silver Nanoparticle Incorporated Titanosilicate ETS-10 Films, in press.*

[12] P. Atienzar, S. Valencia, A. Corma, H. Garcia, *Titanium-Containing Zeolites and Microporous Molecular Sieves as Photovoltaic SolarCells,* Chemical Physical Chemistry, 8, 1115-1119, 2007.

[13] B. Yilmaz, J. Warzywoda, A. Sacco Jr, *Spectroscopic characterization of the quantum wires in titanosilicates ETS-4 and ETS-10,* Institute of Physics publishing, 17, 4092-4099, 2006.

[14] R. Xu, W. Pang, J. Yu, Q. Huo, J. Chen, *Chemistry of Zeolites and Related Porous Materials: Synthesis and Structure*, Wiley, 2007, p 50.

[15] J. A. Incavo, P. K. Dutta, *Zeolite Host-Guest Interactions: Optical Spectroscopic Properties of Tris(bipyridine)ruthenium(II) in Zeolite Y Cages,* Journal of Physical Chemistry, 94, 3075-3081, 1990.

[16] J. Shailaja, P. H. Lakshminarasimhan, Ajit R. Pradhan, R. B. Sunoj, Steffen Jockusch, S. Karthikeyan, S. Uppili, J. Chandrasekhar, N. J. Turro, and V. Ramamurthy, *Alkali Ion-Controlled Excited-State Ordering of Acetophenones Included in Zeolites: Emission, Solid-State NMR, and Computational Studies,* Journal of Physical Chemistry A, 107, 3187-3198, 2003.

[17] R. Xu, W. Pang, J. Yu, Q. Huo, J. Chen, *Chemistry of Zeolites and Related Porous Materials: Synthesis and Structure*, Wiley, 2007, pp:603.

[18] C.J. Lin, T. Yang, C. Lee, S. H. Huang, R. A. Sperling, M. Zanella, J. K. Li, J. Shen, H. Wang, H. Yeh, W. J. Parak, W. H. Chang, *Synthesis, Characterization, And Bioconjugation Of Fluorescent Gold Nanoclusters Toward Biological Labeling Applications*, ACS Nano, 3, 395-401, 2009.

[19] N. Nath, A. Chilkoti. *A colorimetric gold nanoparticle sensor to interrogate biomolecular interactions in real time on a surface*. Analytical Chemistry, *74*: 504–509, 2002.

[20] Y. Mikami, A. Dhakshinamoorthy, M. Alvaro, H. Garcia. *Catalytic activity of unsupported gold nanoparticles*, Catalysis Science & Technology, 3, 58-69, 2013.

[21] S. K. Das, P. K. Dutta. *Synthesis and characterization of a ruthenium oxide–zeolite Y catalyst for photochemical oxidation of water to dioxygen,* Microporous and Mesoporous Materials, 22, 475–483, 1998.

[22] M. Daniel, Didier Astruc. *Gold Nanoparticles: Assembly, Supramolecular Chemistry, Quantum-Size-Related Properties, and Applications toward Biology, Catalysis, and Nanotechnology,* Chemical Reviews, 104: 293-344, 2004.

[23] M..Zahmakıran, S. Özkan, *Intrazeolite Ruthenium(0) Nanoclusters: a Superb catalyst for the Hydrogenation of Benzene and the Hydrolysis of Sodium Borohydride,*Langmuir, 24, 7065-7067, 2000.

[24] K. Lance Kelly, Eduardo Coronado, Lin Lin Zhao, George C. Schatz. The Optical Properties of Metal Nanoparticles: The Influence of Size, Shape, and Dielectric Environment. *The Journal of Chemical Physics B*, 107: 668-677, 2003.

[25] M. Zahmakiran, S. Özkar, *Zeolite-Confined Ruthenium(0) Nanoclusters Catalyst: Record Catalytic Activity, Reusability, and Lifetime in Hydrogen Generation from the Hydrolysis of Sodium Borohydride, Langmuir,* 25, 2667-2678, 2009.

[26] N. Gfeller, G. Calzaferri. *Energy Migration in Dye-Loaded Hexagonal Microporous Crystals,* The Journal of Chemical Physics B, 101, 1396-1408, 1997.

[27] G. Calzaferri, D. Bruhwiler, S. Megelski, M. Pfenniger, M. Pauchard, B. Hennessy, H. Maas, A. Devaux, U. Graf, *Playing with dye molecules at the inner and outer surface of zeolite L.* Solid State Sciences, 2, 421–447, 2000.

[28] R. Xu, W. Pang, J. Yu, Q. Huo, J. Chen, *Chemistry of Zeolites and Related Porous Materials: Synthesis and Structure*, Wiley, 2007, pp:600.

[29] T. A. Ruda-Eberenz, A. Nagy, W. J. Waldman, P. K. Dutta. *Entrapment of Ionic Tris(2,2'-Bipyridyl) Ruthenium(II) in Hydrophobic Siliceous Zeolite:* O_2 *Sensing in Biological Environments,* Langmuir, 24, 9140-9147, 2008.

[30] M. lvaro, J. F. Cabeza, D. Fabuel, A. Corma, H. Garcia. *Electrochemiluminescent Cells Based on Zeolite-Encapsulated Host–Guest Systems: Encapsulated Ruthenium Tris-bipyridyl*, Chemistry: A European Journal, 13, 3733 – 3738, 2007.

[31] S. H. Bossmann, C. Turro, C. Shunabel, M. R. Pokhrel, L. M. Payawan, B. Baumeister, M. Wörner, $Ru(bpy)_3^{2+}/TiO_2$-Codoped Zeolites: Synthesis, Characterization, and the Role of TiO_2 in Electron Transfer *Photocatalysis,* J. Phys. Chem. B, *105*, 5374–5382, 2001.

[32] K. Mori, Y. Kondo, S. Morimoto, H.Yamashita, *Influence of Exchanged Alkali Metal Cations within Zeolite Y Cages on Spectroscopic and Photooxidation Properties of the Incorporated Tris(2,2'-bipyridine)ruthenium(II) Complexes,* J. Phys. Chem. C, 112, 2593–2600,2008.

[33] Y. S. Park, E. J. Lee, Y. S. Chun, Y. D. Yoon, K. B. Yoon, *Influence of Exchanged Alkali Metal Cations within Zeolite Y Cages on Spectroscopic and Photooxidation Properties of the Incorporated Tris(2,22-bipyridine)ruthenium(II) Complexes,* J. Am. Chem. Soc. 2002, *124*, 7123–7135;

[34] P. K. Dutta, W. Turbeville, *Intrazeolitic Photoinduced Redox Reactions between Ru(bpy)*$_3^{2+}$ *and Methyivlologen*, J. Phys. Chem., *96*, 9410–9416, 1992.

[35] N. B. Castagnola, P. K. Dutta, *Nanometer-Sized Zeolite X Crystals: Use as Photochemical Hosts*, Phys. Chem. B, *102*, 1696–1702, 1998.

[36] E. S. Brigham, P. T. Snowden, Y. I. Kim, T. E. Mallouk, *Electron and Energy Transfer as Probes of Interparticle Ion-Exchange Reactions in Zeolite Y*, J.Phys. Chem, *97*, 8650–8655, 1993.

[37] R. Xu, W. Pang, J. Yu, Q. Huo, J. Chen, *Chemistry of Zeolites and Related Porous Materials: Synthesis and Structure*, Wiley, 2007, pp:611.

[38] W. H. Quayle, J. H. Lunsford, *Tris(2,2'Bipyridine)ruthenium(III) in Zeolite Y: Characterization and Reduction on Exposure to Water*, Inorg. Chem, *21*, 97-103, 1982.

[39] N. Taira, M. Saitoh, S. Hashimoto, H. R. Moon, K. B. Yoon, *Effect of electron-acceptor strength of zeolite on the luminescence decay rate of Ru(bpy)*$_3^{2+}$ *incorporated within zeolites*, Photochem. Photobiol. Sci., *5*, 822–827, 2006.

[40] Z. Ji, J. Warzywoda, A. Sacco Jr., *Synthesis and morphological control of large titanosilicate ETS-10 crystals*, Microporous and Mesoporous Materials, 109, 1–11, 2008.

[41] S. J. Datta, K. B. Yoon, *Synthesis of large monodisperse ETS-10 crystals and observation of quantum confinement effects from very long titanate quantum wires*, Catalysis Today, 204, 60-65, 2013.

[42] M. W. Anderson, J. R. Agger, N. Hanif, O. Terasaki, T. Ohsuna, *Crystal growth in framework materials*, Microporous and Mesoporous Materials, 48, 1-9, 2001.

[43] Y. Zhu, Z. Hua, J. Zhou, L. Wang, J. Zhao, Y. Gong, W. Wu, M. Ruan, J. Shi, *Hierarchical Mesoporous Zeolites: Direct Self-Assembly Synthesis in a Conventional Surfactant Solution by Kinetic Control over the Zeolite Seed Formation*, Chemistry A European Journal, 17, 14618 – 14627, 2011.

[44] S. Wang, T. Dou, Y. Li, Y. Zhang , X. Li, Z. Yan. *A novel method for the preparation of MOR/MCM-41 composite molecular sieve*. Catalysis Communications, 6, 87-91, 2005.

[45] X. Yang, Y. Feng, G. Tian, Y. Du, X. Ge, Y. Di, Y. Zhang, B. Sun, F. Xiao, *Design and size control of uniform zeolite nanocrystals synthesized in adjustable confined voids formed by recyclable monodisperse polymer spheres*, Angew. Chem., Int. Ed., 44, 2563-2568, 2005.

[46] M. Hartmann, *Hierarchical zeolites: a proven strategy to combine shape selectivity with efficient mass transport*, Angew. Chem., Int. Ed., 43, 5880, 2004.

[47] J.L. Motz, H. Heinichen, W.F. Holderich, *Direct hydroxylation of aromatics to their corresponding phenols catalysed by H-[Al]ZSM-5 zeolite*, Journal of Molecular Catalysis A: Chemical 136, 175–184, 1998.

[48] M. Ogura,S. Shinomiya, J. Tateno, Y. Nara, E. Kikuchi, M. Matsukata, *Formation of uniform mesopores in ZSM-5 zeolite through treatment in alkaline solution*. Chem. Lett. 2000, 882.

[49] J.C. Groen, L.A.A. Peffer, J.A. Moulijn, J. Perez-Ramırez, *On the introduction of intracrystalline mesoporosity in zeolites upon desilication in alkaline medium,* Microporous Mesoporous Mater. 2004, 69, 29.

[50] I. Schmidt, A. Boisen, E. Gustavsson, K. Ståhl, S. Pehrson, S. Dahl, A. Carlsson, C. J. H. Jacobsen, *Carbon Nanotube Templated Growth Of Mesoporous Zeolite Single Crystals*. Chem. Mater. 2001, 13, 4416.

[51] C. H. Christensen, K. Johannsen, I. Schmidt, C. H. Christensen, *Catalytic Benzene Alkylation Over Mesoporous Zeolite Single Crystals: İmproving Activity And Selectivity With A New Family Of Porous Materials.* J. Am. Chem. Soc. 2005, 44, 13370.

[52] S. Lingling, L. Lin, J. Zhuang, H. Wang, Y. Li, W. Shen, Y. Xu, X. Bao, *Creating mesopores in ZSM-5 zeolite by alkali treatment: a new way to enhance the catalytic performance of methane dehydroaromatization on Mo/HZSM-5 catalysts,* Catalysis Letters Vol. 91, 3–4, 2003.

[53] M. W.Anderson, J. R. Agger, N. Hanif, O. Terasaki, T. Ohsuna, T., *Crystal growth in framework materials*, Solid State Sci. 2001, *3*, 809.

[54] C. C. Pavel, *Structural Defects Induced in ETS-10 by Postsynthesis Treatment with H2O2 Solution*, Chem. Mater. 2006, *18*, 3813-3820.

[55] G. Koermer, A. Thangaraj, S. Kuznicki, Studies in Surface Science and Catalysis Volume, Stud. Surf. Sci. Catal. 135 (2001) 1619.

[56] F.X. Llabre´s i Xamena, P. Calza, C. Lamberti, C. Prestipino, A. Damin, S. Bordiga, E. Pelizzetti, A. Zecchina, Enhancement of the ETS-10 Titanosilicate Activity in the Shape-Selective Photocatalytic Degradation of Large Aromatic Molecules by Controlled Defect Production , J. Am. Chem. Soc. 125, 2264,2003

[57] Z. Ji, D. M. Callahan Jr., M. N. Ismail, J. Warzywoda, A. Sacco Jr., *Development and characterization of a titanosilicate ETS-10-coated optical fiber reactor towards the photodegradation of methylene blue,* Journal of Photochemistry and Photobiology A: Chemistry, 217, 22-28, 2011.

[58] M. Zahmakıran, S. Özkan, *Zeolite Confined Nanostructured Dinuclear Ruthenium Clusters: Preparation, Characterization And Catalytic Properties İn The Aerobic Oxidation Of Alcohols Under Mild Conditions* , J. Mater. Chem., 2009, 19, 7112–7118.

[59] B.M. Faroldi, E.A. Lombardo, L.M. Cornaglia, S. Irusta, *Application of ETS-10 Microporous titanosilicate as support of Ru nanoparticles for hydrogen production,* Applied Catalysis A: General 417– 418 (2012) 43– 52.

[60] W. DeWilde, G. Peeters, J. H. Lunsford, *Synthesis and Spectroscopic Properties of Tris(2,2'-bipyridine)ruthenium(II) in Zeolite Y,* J. Phys. Chem. 1980, *84*, 2306-2310

[61] G. Calzaferri, N. Gfeller, *Thionine in the Cage of Zeolite L,* Journal of Physical Chemistry, 96, 3428-3435, 1992.

[62] S. Cox, T. Gier, G. Stucky, J. Bierlein, *Inclusion Tuning Of Nonlinear Optical-Materials - Switching The Shg Of Para-Nitroaniline And 2-Methyl-Para-Nitroaniline With Molecular-Sieve Hosts,* Journal Of The American Chemical Society, 110, 2986-298, 1988.

[63] S. Wohlrab, *Encapsulation of methylene blue into aluminophosphate family molecular sieves,* Zeolites**,** 12, 862–865, 1992.

[64] C. Xu, D. Mochizuki, Y. Hashimoto, T. Honda, Y. Tsukahara, T. Yamauchi, Y. Wada, *Luminescence of ortho -Metalated Iridium Complexes Encapsulated in Zeolite Supercages by the Ship-in-a-Bottle Method*, Eur. J. Inorg. Chem. 2012, 3113–3120

[65] P. Laine, M. Lanz, G. Calzaferri, *Limits of the in Situ Synthesis of Tris(2,2-bipyridine)ruthenium(II) in the Supercages of Zeolite Y*, Inorg. Chem. 1996, *35*, 3514-3518.

[66] G. Ihlein, F. Schuth, O. O. Krauss, U. Vietze, F. Laeri, *Alignment of a laser dye in the channels of the $AlPO_4$-5 molecular sieve,* Advanced Materıals, 10, 1117, 1998.

[67] P. Yang, G. Wirnsberger, H. Huang, S. Cordero, M. McGehee, B. Scott, T. Deng, G. Whitesides, B. Chmelka, S. Buratto, G. Stucky, *Mirrorless lasing from mesostruuctured waveguides patterned by soft lithography,* SCIENCE, 287, 465-467,2000.

[68] G. Wirnsberger, G. D. Stucky, *Microring Lasing from Dye-Doped Silica/ Block Copolymer Nanocomposites,* Chem. Mater. 2000, *12*, 2525-2527

[69] R. Vogel, *Mesostructured Dye-Doped Titanium Dioxide for Micro-Optoelectronic Applications*, Chemical Physical Chemistry, 2003, 4, 595-603

[70] K. Rurack, K. Hoffmann, W. Al-Soufi, U. Resch-Genger, *2,2 '-bipyridyl-3,3 '-diol incorporated into AlPO4-5 crystals and its spectroscopic properties as related to aqueous liquid media,* Journal Of Physıcal Chemıstry B, 106, 9744-9752, 2002.

[71] R. A. Van Santen, *Physical chemistry: Porous solids get organized, Nature* 444, 46-47, 2006.

[72] G. Calzaferri, *Organizing supramolecular functional dye-zeolite crystals*

Unidirectional antenna systems, 23rd European Crystallographic Meeting, Leuven 6-11 August 2006.

[73] M. M. Yatskou, M. Meyer, S. Huber, M. Pfenniger, G. Calzaferri, *Electronic Excitation Energy Migration in a Photonic Dye-Zeolite Antenna,* Chemical Physical Chemistry, 2003, 4, 595-603

[74] M. Pauchard, S. Huber, R. Allet-Renault, H. Maas, R. Pansu, G. Calzaferri, *Time- and Space-Resolved Luminescence of a Photonic Dye - Zeolite Antenna*, Angew. Chem. Int. Ed., 40, 15,2001.

[75] L. Lv, F. Su, X.S. Zhao, *A reinforced study on the synthesis of microporous titanosilicate ETS-10*, Micropor. Mesopor. Mater. ,76, 113, 2004.

[76] P. Wu, T. Tatsumi, T. Komatsu, T. Yashima, *A Novel Titanosilicate with MWW Structure. I. Hydrothermal Synthesis, Elimination of Extraframework Titanium, and Characterizations*, J. Phys. Chem. B**,** *105*, 2897-2905, 2001.

[77] J.P. Marques, I. Gener, P. Ayrault, *Infrared spectroscopic study of the acid properties of dealuminated BEA zeolites*, Microporous and Mesoporous Materials 60 (2003) 251–262.

[78] Y. Lee, J. S. Lee, K. B. Yoon, *Synthesis of long zeolite-L crystals with flat facets*, Microporous and Mesoporous Materials, 80, 237–246, 2005.

[79] H. Maas, G. Calzaferri, *Trapping Energy from and Injecting Energy into Dye - Zeolite Nanoantennae*, Angew. Chem. Int. Ed. 2002, 41, 13

[80] D. Bruhwiler, G. Calzaferri, *Molecular sieves as host materials for supramolecular organization*, Microporous and Mesoporous Materials 72 (2004) 1–23

[81] St. Huber, G. Calzaferri, *Light-harvesting host-guest antenna materials for solar energy conversion devices, Photonics for Solar Energy Systems*, edited by Andreas Gombert, Proc. of SPIE Vol. 6197, 619708, (2006)

[82] M. Zahmakıran, S. Özkan, *Zeolite Confined Nanostructured Dinuclear Ruthenium Clusters: Preparation, Characterization And Catalytic Properties In The Aerobic Oxidation Of Alcohols Under Mild Conditions* , J. Mater. Chem., 2009, 19, 7112–7118.

[83] N. Gfeller, S. Megelski, G. Calzaferri, *Transfer of Electronic Excitation Energy between Dye Molecules in the Channels of Zeolite L*, J. Phys. Chem. B, 102, 14, 1998.

[84] J. Rocha, A. Ferreira , Zhi Lin, M. W. Anderson, *Synthesis of microporous titanosilicate ETS-10 from $TiCl_3$ and TiO_2: a comprehensive study,* Microporous and Mesoporous Materials 23 (1998) 253–263

[85] S. Galioğlu, Synthesis and Characterization of Titanosilicate ETS-10 for Potential Photovoltaic Applications. MS Thesis, 2010,pp.39

[86] T. K. Das, S. Sivasanker, *Preparation, Characterization and Catalytic Properties of the Microporous Titanosilicate, ETS-10,* Bull. Mater. Sci. , 17, 1143-1153, 1994.

[87] M. W. Anderson, O. Terasaki, O. Ohsuna, P.J. O'Malley, A. Philippou, S.P. MacKay, A. Ferreira, J. Rocha, S. Lidin, Philos. Mag. B, 71, 813-841, 1995.

[88] P. Calza, C. Pazé, E. Pelizzetti, A. Zecchina, *Shape-selective photocatalytic transformation of phenols in an aqueous Medium,* Chem. Commun., 2130–213, 2001.

[89] P. Li, W. Su, J. Cui, L. Huo, N. Guo, Y. Huang, *Computer Simulation of Ruthenium Complexes Molecules: Density Functional Theory Study of Ruthenium Tris Chelate Complexes,* 2011 International Conference on Computer Science and Information Technology (ICCSIT 2011), IPCSIT, vol. 51, 2012.

APPENDIX A

SCANNING ELECTRON MICROSCOPY IMAGES OF POST-TREATED SAMPLES

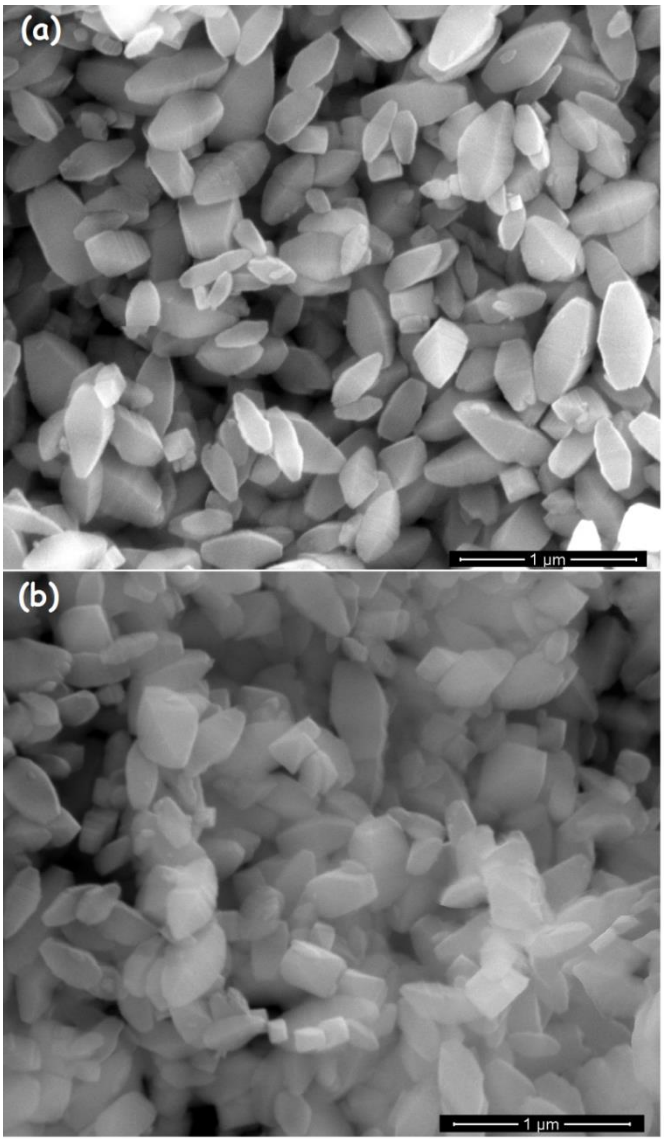

Figure A. 1. SEM images of N-ETS-10-30%(1) and N-ETS-10-30%(1)-S.

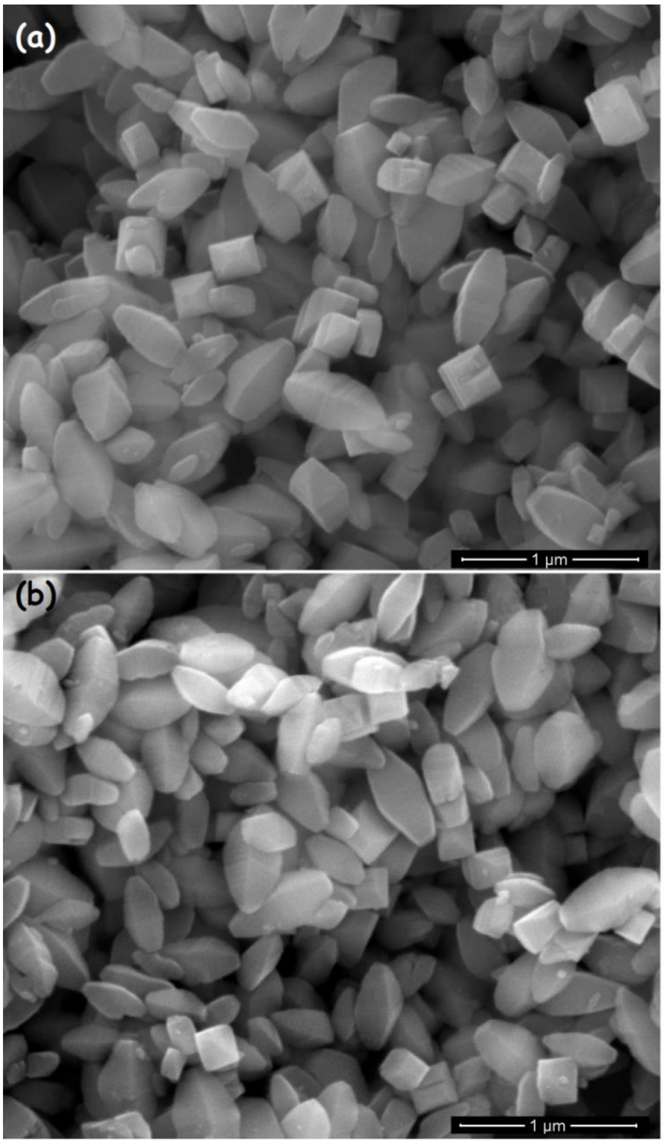

Figure A. 2. SEM images of N-ETS-10-10%(3) and N-ETS-10-10%(3)-S.

APPENDIX B

RAMAN SPECTRA

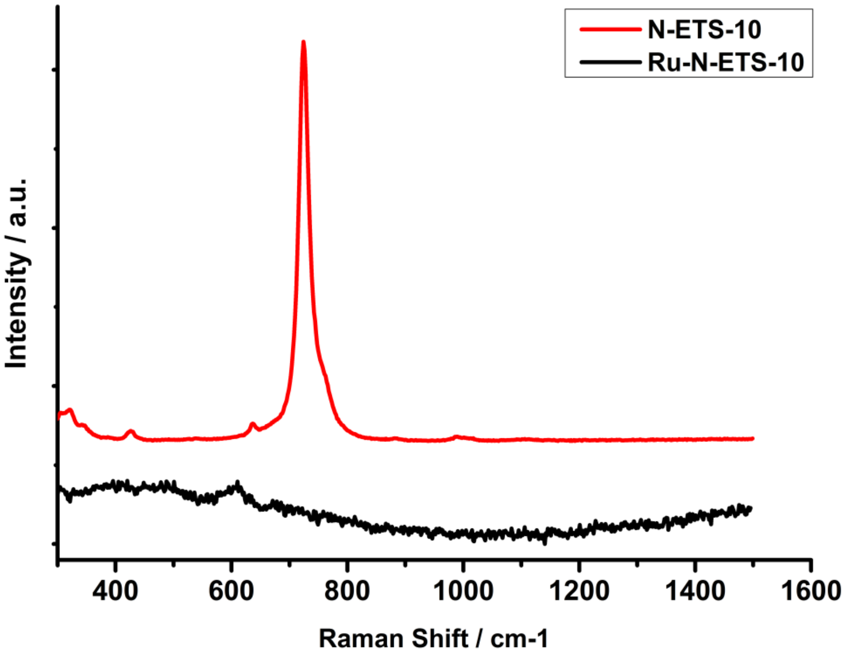

Figure B.1. Raman Spectra of N-ETS-10 and Ru-N-ETS-10

APPENDIX C

UV-VIS SPECTRUM

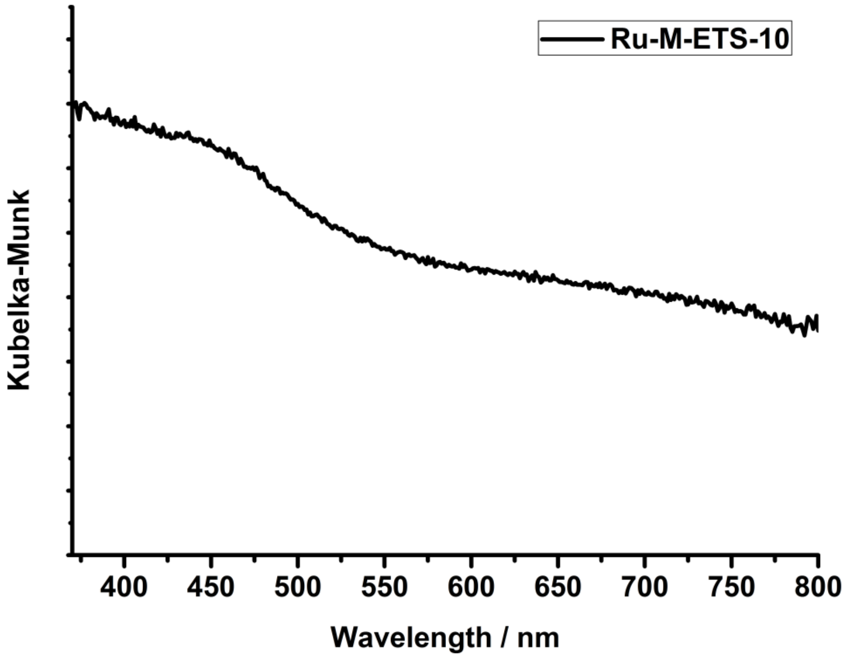

Figure C.1. UV-Vis spectrum of Ru-M-ETS-10.